# Aerodynamic Design of Centrifugal Compressor for Heavy Duty Truck Applications

Amanda Karlsson

Dedicated to Assar Karlsson.
1936–2017

*“Got dat manná, morfar”.*

# Abstract

The transport sector is one of many markets facing new challenges in the pursuit of reduced greenhouse gas emissions. The people at Volvo Powertrain in Malmö are continuously working to develop new and improved techniques that are able to live up to the ever-increasing legislations. A well performing turbocharger is an essential part of the combustion engine in order to reduce the fuel consumption and $CO_2$-emissions. The engineers of today have powerful tools at their disposal that help them with the task of designing, developing and analysing these kinds of components. Advanced calculations such as CFD can be performed thanks to the great computational power of computers, a task that would seem impossible by hand.

These tools have been used to create a new design for one of Volvo's in-house turbo compressors for heavy duty vehicle application, with the purpose of improving the performance. The parts of the compressor that were subject to the design update are the impeller and diffuser.

The in-house-compressor was first analysed in three operating points in the CFD-simulation program *Star-CCM+*. These results would constitute the benchmark for the new design. Using the in-house-compressor design as a starting point, new designs for the impeller and diffuser were made using the software package *TURBOdesign Suite*. The new impeller design was then put through iterations of optimizations in *TURBOdesign* and CFD-simulations in *Star-CCM+* in the same three operating points as the in-house-compressor. The new diffuser design didn't go through any optimizations. The results from the CFD-simulations of the final new impeller and diffuser designs were finally compared to those of the in-house-compressor to discern the differences in performance between the two designs.

The new design displays higher efficiencies in all three operating points, with the biggest improvement in the design point where the efficiency is 1.8%-points higher. The flow analysis shows that the new design has more even flows; it however doesn't achieve as high flows as the in-house-compressor. One explanation for this may be the more tangential diffuser vanes of the new diffuser design. Consequently, the diffuser of the in-house-compressor performs better than the new one in the high operating point (high mass flow).

The leading edge of the impeller blades were found to be a bit too thin in the stress and vibration analyses in order to pass the criterion that Volvo has on the strength of the blade with regards to the eigenfrequency.

Future studies may want to look into further designs of the diffuser vane since only one new diffuser design was tested together with the new impeller. This could lead to achieving higher flow rates. Furthermore, the leading edge of the impeller blade should be made thicker in order to pass the strength criteria. Since this can lead to a slightly smaller throat area in the impeller this alteration should be accompanied by

adjustments to counteract this, for example a reduction of the blade and meridional hub angle at the inlet.

# Sammanfattning

Transportindustrin är en av många marknader som ställs inför nya utmaningar i jakten på reducerade utsläpp av växthusgaser. På Volvo Powertrain AB i Malmö pågår ständigt arbete med att utveckla nya och förbättrade tekniker för att möta de nya kraven. En viktig komponent för att kunna reducera bränsleförbrukningen och därmed $CO_2$-utsläppen från en förbränningsmotor är en högpresterande turbo. Till sin hjälp har dagens ingenjörer kraftfulla verktyg i sitt förfogande i arbetet med att designa, utveckla och analysera komponenter av detta slaget. Med den räknekraft som datorer innebär kan avancerade beräkningar som CFD genomföras, något som skulle te sig nästintill omöjligt för hand.

Dessa verktyg har använts för att ta fram en ny design på en av Volvos in-house turbo-kompressorer, med målet att förbättra dess prestanda. De komponenter av kompressorn som varit föremål för designuppdateringen är rotorn och diffusorn.

In-house-kompressorn analyserades först i tre driftpunkter i CFD-simuleringsprogrammet *Star-CCM+*. Resultaten från dessa simuleringar utgjorde utgångsvärden som den nya designen fick förhållas till. En ny design av rotor och diffusor arbetades fram i programpaketet *TURBOdesign Suite*, med utgångspunkt i designen hos in-house-kompressorn. Den nya rotordesignen genomgick sedan iterationer av optimeringar i *TURBOdesign* och CFD-simuleringar i *Star-CCM+* i samma tre driftpunkter som in-house-kompressorn. Den nya diffusordesignen genomgick inga optimeringar. Resultaten från CFD-simuleringarna av den slutgiltiga designen med ny rotor och diffusor jämfördes således med resultaten från in-house-kompressorn för att avläsa skillnader i prestanda mellan de två designerna.

Den nya designen visar på högre verkningsgrad i alla tre driftpunkter, med störst skillnad i designpunkten där verkningsgraden är 1.8% högre. Flödesanalysen visar på jämnare flöden genom den nya designen, den uppnår dock inte lika höga massflöden som in-house-kompressorn, en förklaring till detta kan vara de mer tangentiella diffusorbladen i den nya diffusorn. Följaktligen så presterar den gamla diffusorn bättre än den nya i driftpunkten med högst belastning (högt massflöde).
Vid spännings- och vibrationsanalyser av den nya designen framgick det att framkanten av rotorbladet är lite för tunn för att klara av de kriterier som Volvo ställer på hållfastheten med avseende på egenfrekvensen.

I framtiden kan det vara intressant att kolla på ytterligare versioner av diffusorblad då endast en design testades med den nya rotordesignen. Detta skulle kunna medföra att högre massflöden kan tillåtas. Fortsättningsvis bör framkanten av rotorbladen göras tjockare för att klara av de krav som ställs på hållfastheten. Då detta kan orsaka något mindre chokearea i rotorn bör en sådan ändring ackompanjeras av justeringar för att motverka detta, förslagsvis en mindre blad- och hubbvinkel i inloppet.

# Acknowledgements

This thesis has been conducted in the spring of 2018 at the Department of Energy Sciences, Faculty of Engineering, LTH, Lund University, and at Volvo Powertrain AB in Malmö as part of my degree of Master of Science in Engineering.

I would like to express my gratitude to my supervisor at Lund University, Magnus Genrup, for all his help and advice, as well as his enthusiasm and for putting me into contact with the people at Volvo Powertrain AB to begin with.

A special thank you to my supervisor at Volvo Powertrain AB, Magnus Ising, for his unfaltering guidance and teachings along the way. I have learnt a lot from you and I felt like I was in very secure hands from the very start. My appreciation also goes out to Martin Bauer the engine performance analysis group manager at Volvo for giving me the opportunity to do my master thesis for a company that I hold in high regards and making me feel like the work is of value. Thank you to Håkan Torstensson for his work in creating CAD-models and performing stress analyses.
I would also like to thank the rest of the employees at Volvo, for making me feel welcome and like a part of your team.

Finally, a big thank you to my family and friends for their continued support and encouragements, without whom this work would not have been possible.

Lund, June 2018

Amanda Karlsson

# Nomenclature

| **Symbol** | Unit | Description |
|---|---|---|
| a | [m/s$^2$] | Acceleration |
| C | [m/s] | Absolute flow velocity |
| $c_p$ | [J/kg K] | Specific heat capacity, constant pressure |
| $c_v$ | [J/kg K] | Specific heat capacity, constant volume |
| E | [J] | Energy |
| F | [N] | Force |
| g | [m/s$^2$] | Gravitational acceleration |
| h | [J/kg] | Specific enthalpy |
| I | [J/kg] | Rothalpy (Trothalpy) |
| m | [kg] | Mass |
| p | [Pa] | Pressure |
| P | [W] | Power |
| Q | [J] | Heat |
| r | [m] | Radius |
| R | [J/kg K] | Specific gas constant |
| t | [s] | Time |
| T | [K] | Temperature |
| u | [J] | Internal energy |
| U | [m/s] | Blade speed |
| v | [m/s] | Velocity |
| $v$ | [m$^3$/kg] | Specific volume |
| W | [m/s] | Relative flow velocity |
| W | [J] | Work |
| z | [m] | Height |
| | | |
| $\delta$ | | Partial derivative |
| $\eta$ | | Efficiency |
| $\Omega$ | [rad/s] | Angular velocity |
| $\theta$ | [J] | Flow energy |
| $\rho$ | [kg/m$^3$] | Density |
| $\tau$ | [Nm] | Torque |

## Subscripts

| **Symbol** | Description |
|---|---|
| $\theta$ | Tangential velocity component |
| r | Radial velocity component |
| 0 | Stagnation or total state |

## Superscripts

| **Symbol** | Description |
|---|---|
| $\cdot$ | Rate form |

# Contents

# Chapter 1

## Introduction

The name Volvo has its origin in 1911, when the Swedish bearings company SKF registered it as a trademark. It was supposed to be the name of a series of ball bearings but was never used as such. Volvo as a car company was more accurately founded in 1927 by Assar Gabrielsson and Gunnar Larsson, when the first car was built in their factory on Hisingen in Gothenburg, Sweden. The first Volvo truck was produced the following year and it was an instant success.

Volvo has since then grown significantly and gone through many changes through the years. SKF sold their shares in 1935 when AB Volvo was introduced to the stock exchange market. In 1978 the car division of Volvo was split into a separate company within the Volvo Group and was eventually sold to Ford Motor Company in 1999 (James, 2016).

Today, Volvo Group is a global manufacturer of commercial vehicles such as trucks, buses, construction equipment, and marine engines. They employ around 100 000 people world-wide, operate in 190 markets and have production facilities in 18 countries.

Volvo Group Trucks Technology is the global truck technology and development organization within Volvo Group. They in turn employ about 7 000 people, mostly engineers, which are in charge of the technology research, and product development and design within Volvo Group. The offices in Malmö are part of the Powertrain Engineering branch, responsible for the development of the engines and its support technologies such as turbochargers and exhaust after treatment systems (EATS) for the brands within Volvo Group.

## Background

The transport sector is a big contributor of large amounts of $CO_2$-emissions. Globally this sector was responsible for 24% of the total $CO_2$-emissions in 2015; in Sweden the number was around 30% in 2017 (International Energy Agency, 2017) (Dickinson, 2017). $CO_2$ is the number one anthropogenic greenhouse gas (GHG), constituting around 76% of the total anthropogenic GHG's (III, 2014). The main source of these emissions is the burning of fossil fuels.

Greenhouse gases are thus called because of their contribution to the greenhouse effect. These gases absorb heat radiation in the form of infrared light reflected from the surface of the earth's lands and oceans. The heat absorbed is slowly released back into the atmosphere. This is known as the greenhouse effect. Without it, the average

temperature at earth's surface would be around -18° C, compared to the actual +15° C.

$CO_2$ is a naturally occurring gas in the earth's atmosphere, however, since the industrial revolution the amount of $CO_2$ has increased from 280 ppm to around 400 ppm today. This increase in atmospheric $CO_2$ has been accompanied by a 1° C increase in the earth's average surface temperature. A continued rise in the concentration of $CO_2$ and other GHG's is projected to a have an impact on the climate and various biological and ecological systems, including sea-level rise, loss of habitat leading to a decrease in biological diversity, an increase in extreme weather phenomena, and loss of arable land. All of which could mean potential mass emigrations with consequences far beyond imagining.

Efforts to reduce and limit the exploitation of fossil fuels and emissions of GHG's are constantly being made. The Kyoto protocol that was active between 2008 and 2012 was an international agreement between 192 nations that committed the participating parties to *"...pursue limitation or reduction of emissions of greenhouse gases..."* (United Nations, 1998). In 2015 the Paris Agreement was negotiated between 196 parties at the United Nations Climate Change Conference. The goal of the agreement, which is to be taken into effect in 2020, is to keep the average temperature increase well below 2° C compared to pre-industrial levels by means of GHG-emissions mitigation (United Nations, 2015).

The EU has adopted directives in the form of European emission standards which regulate the allowed emission levels for new vehicles sold within the EU and the EEA. These emission standards do not control $CO_2$-emissions, but the emissions of $NO_x$, CO, particle matter (PM), total hydrocarbons (THC), and non-methane hydrocarbons (NMHC), which are all produced by vehicles running on fossil fuels. These directives are rolled out continually with progressively increasing standards.

Volvo Group is taking an active part in pushing the development of smarter and cleaner technologies to meet these ever-restricting criterions on emission regulation.

## 1.1 Purpose

To achieve reduced fuel consumption and $CO_2$-emissions in a combustion engine, a well performing turbocharger is an essential part.

Volvo Powertrain AB has an in-house design on a centrifugal compressor for heavy duty vehicle application, hereafter referred to as *in-house-compressor*. The in-house-compressor is a centrifugal turbo compressor fashioned with a vaned diffuser and ported shroud for range extension. It is designed for a relatively high pressure ratio and displays good performance and efficiency levels; it was however designed some time ago. Volvo has since then acquired new design- and development software for these types of components. It might therefore be possible to improve the performance of the unit by updating the design of the compressor with the help of these new tools – and thereby achieve lower fuel consumption and reduced $CO_2$-emissions.

## 1.2 Focus

The parts of the centrifugal compressor that are subject to the design update are the impeller and the vaned diffuser. Any performance improvements will most likely be made in the design of these components since they have the biggest impact on the operation of the compressor. Remaining parts such as volute and ported shroud are not included in the design update; neither is any necessary CAD-modeling, structural, or solidity analyses of any of the parts, these will instead be carried out and provided by Volvo to aid in the design process.

## 1.3 Problem Statement

Is it possible to improve the performance of the centrifugal in-house-compressor by updating the design of the impeller and diffuser with the help of the tools available?

## 1.4 Tools

The following programs will be used to aid in this work:

- *Star-CCM+ 12.06.010* by Siemens – CFD-simulation program
- *TURBOdesign Suite v6.4.0* by Advanced Design Technology (ADT) – 3D turbomachine design, optimization, and analysis program

# Chapter 2

# Method

*The work procedure and methods used to find an answer to the problem statement is presented in this chapter. A quantitative research method has been used in the work towards achieving an improved design for the in-house-compressor, and consisted largely of three parts:*

- *Analysis of the in-house-compressor*
- *Rendering and optimization of new design*
- *Analysis of new design*

*The last two parts were performed in an iterative manner until a satisfactory design was found, or for as long as the allotted time would allow. The software listed under chapter* 1. 4 Tools *were utilized throughout these steps.*

## 2.1 Quantitative Method

A quantitative research method has been used in the pursuit of improving the performance of the in-house-compressor. A quantitative research is performed by way of objective measurements, and structural, mathematical analysis of gathered data (University of Southern California, 2018). The tools used to go by this were the two sets of computer programs under chapter *1.4 Tools*: One for aerodynamic 3D design and optimization of turbomachines, and the other a Computational Fluid Dynamics, CFD, simulation software.

*Star-CCM+* by Siemens was used to perform the CFD-simulations and design analyses in accordance to part one and three in the work procedure described above, while *TURBOdesign Suite* was used in rendering and optimizing the new compressor design in accordance to part two.

### 2.1.1 CDF – Computational Fluid Dynamics

Computational Fluid Dynamics, or CFD, is a way of analyzing a process or system involving a flow of a medium and heat transfer, along with their related phenomena, by way of computer-based simulations. CFD is a powerful tool that is used more and more throughout a number of areas of application, Versteeg and Malalasekera list a couple of examples, some of which are: aerodynamics of aircraft and vehicles, hydrodynamics of ships, power plants: combustion in IC engines and gas turbines, turbomachinery: flows inside rotating passages, diffusers etc., and meteorology: weather prediction (Versteeg & Malalasekera, 1995). CFD is a cost effective and time

efficient way of testing various components and systems, there is no manufacturing involved and thus no material costs, except for the license of the software.

## 2.2 Implementation

*The steps taken to find an answer to the problem statement with the help of the aforementioned method and tools are described in the following chapters.*

### 2.2.1 Analysis of the In-House-Compressor

Before an approach towards a new design can be taken, the existing one must first be examined and evaluated. The first step therefore consisted of setting up the model of the in-house-compressor in *Star-CCM+* and then perform CFD-simulations in a number of operating points. The results from these simulations established the benchmark for the new design.

***Figure 1.*** *The complete model of the in-house-compressor in Star-CCM+.*

The simulations of the in-house-compressor were performed on a complete model consisting of all parts from inlet to volute, as well as on two sector models. The two sector models comprise one with a vaned diffuser and one with a vaneless diffuser, both with the volute and ported shroud excluded. The sector model with the vaned diffuser is made up of $1/8^{\text{th}}$ sectors of the impeller and inlet, and a $1/10^{\text{th}}$ sector of the diffuser.

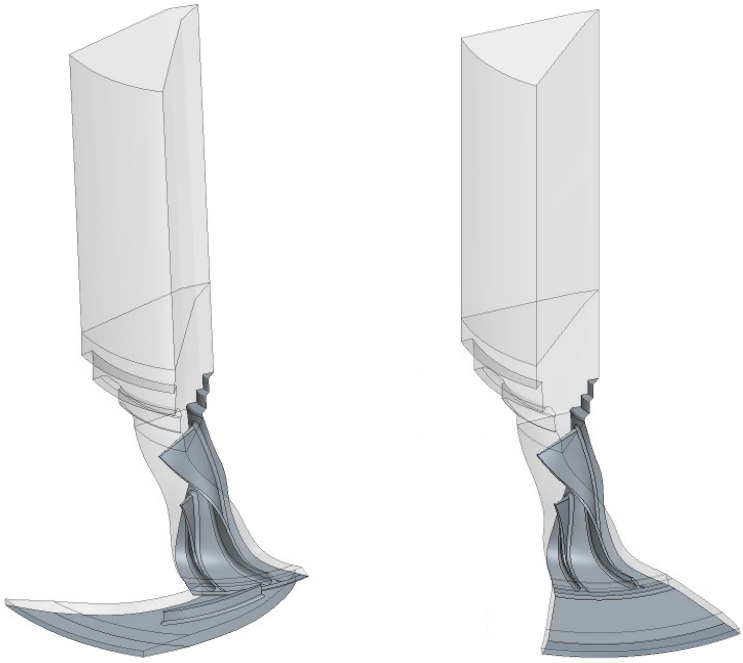

***Figure 2.*** *The vaned (left) and vaneless (right) sector models of the in-house-compressor in Star-CCM+.*

The difference in sector division between impeller and diffuser stems in the fact that the impeller has eight full blades and eight splitter blades, while the diffuser has ten vanes. The sector model with the vaneless diffuser thus consists of $1/8^{\text{th}}$ sectors of all three parts; inlet, impeller, and diffuser. It was used to compare the impeller performance of the in-house-compressor to the new impeller designs, while the vaned diffuser model was used to compare the performance of the impeller and diffuser together. The reason for performing the simulations of the in-house-compressor on sector models in addition to the complete one was the considerable reduction in the simulation time this offered. It made the analysis process more efficient since it made it possible to also simulate the draft designs as sector models. The simulations of the complete model of the in-house-compressor did not only constitute a benchmark for the complete model of the new design but was also a means to make sure that the results from the sector model simulations didn't deviate too much from the actual case.

Each model (complete and sector, vaned and vaneless) were simulated at three operating points respectively. An operating point is defined by the pressure ratio, the constant rotational speed, and the corrected mass flow. The operating points selected for the simulations are marked in *Figure 3. Compressor map with the three selected operating points marked in yellow.*

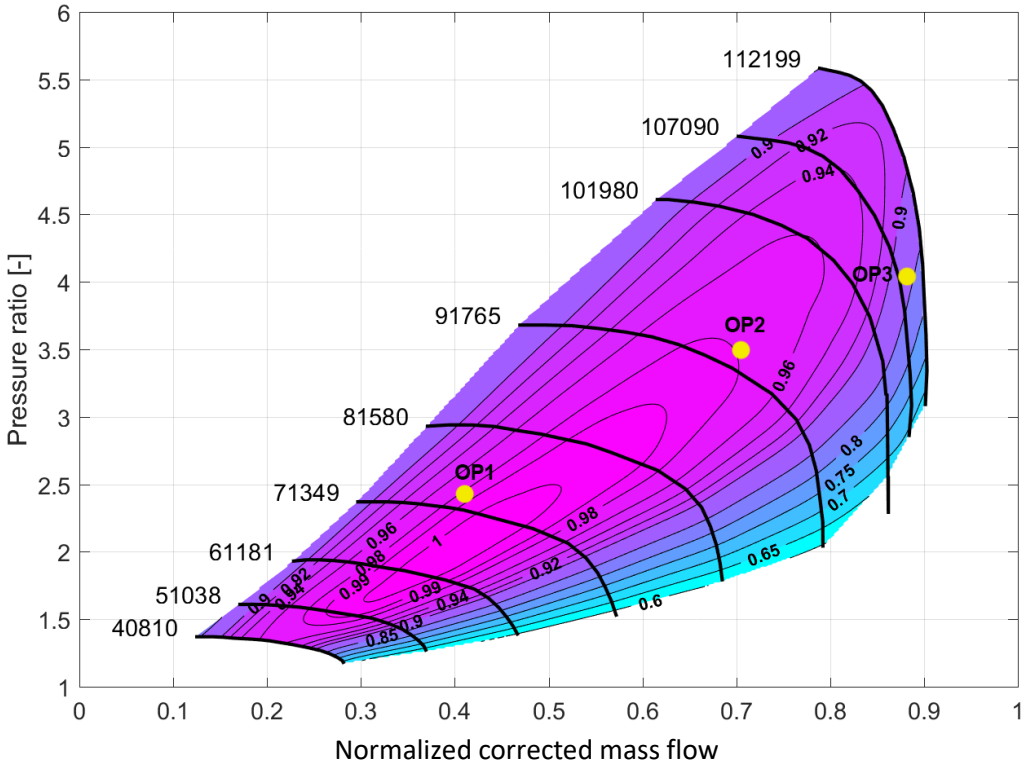


***Figure 3.*** *Compressor map with the three selected operating points marked in yellow.*

This is not the actual map of the in-house-compressor; the efficiency islands and the x-axis containing the corrected mass flow have both been normalized. It is however useful in displaying the areas of the map in which the chosen operating points are located. The three points are the design point (OP2) of the in-house-compressor, a part load point (OP1), and a high load point (OP3). Together they cover interesting portions of the compressor map. The design point is important to test for since a replacement should be designed for the same operating conditions. The part load point is located in an area of the map where the in-house-compressor often operates. It also incorporates conditions closer to surge, while the high load point exemplifies operation near choke conditions.

#### 2.2.1.1 CFD-Model

The CFD-model of the in-house-compressor differs somewhat from the physical model. Since the design of this compressor, an abradable coating on the shroud surface has been taken into use, which allows for minor contact between the shroud and impeller blades. This means that a new design with this coating can be given a smaller tip clearance than that of the in-house-compressor. So in order to make the comparison more just, the CFD-model of the in-house-compressor was given the same constant tip clearance as the new design, one of 0.25 mm, which is considered appropriate if not conservative for use with an abradable coating. Any possible performance improvement in the new design would then depend on the design of the impeller and/or diffuser, rather than the reduced tip clearance. As small a tip

clearance as possible is desired, since this minimizes tip leakage. The actual tip-clearance of the in-house-compressor is somewhere between 0.35-0.40 mm.

Furthermore, the cavity between the impeller hub and the diffuser plate as well as the backface cavity have been removed and replaced by a smooth continuation of the hub to make for more stable simulations. The fillets of the impeller blades were given a constant radius, whereas the actual compressor has a varying fillet radius with increasing size towards the trailing edge suction surface. The inlet is modeled as a simple pipe that has been extended to ensure good uniform flow conditions at the inlet boundary. The pipe diameter is 104 mm and the length is 190 mm. For the complete model, the outlet of the volute has also been extended for the same reason, to a length of 200 mm.

The CFD-model is made up of the air volume within the compressor parts since the CFD-simulations are performed on the flow through the machine, rather than on the machine itself.

#### 2.2.1.2 Preparing the Model in Star-CCM+

The CDF-simulations and analyses were carried out in the Siemens program *Star-CCM+ 12.06.010*. The air geometry of the in-house-compressor was imported from step- and parasolid files for each compressor part, (inlet, impeller, and diffuser for the sector models, and ported shroud, and volute additionally for the complete model). Each of these parts consisted of one big surface respectively. These were divided into smaller surfaces in order to be able to perform calculations on select parts later on and to specify boundary conditions, as well as to be able to define which surfaces of the compressor are static and which are rotating. This division also makes it possible to define the mesh differently for different surfaces, meaning that bigger, simpler surfaces can be assigned a larger mesh, while smaller and more detailed ones can be assigned a finer mesh. This helps reduce the number of total cells and the size of the file, which makes the simulation more efficient while not sacrificing the refinement needed in the more detailed areas of both the geometry and the flow.

The next step was to define the mesh for the model. The mesh divides the entire model into millions of small volumetric cells. Each cell has its physiological condition and during the simulation a solution describing this condition is calculated within each cell.

A polyhedral mesh with ten prism layers at the walls, with a stretching of 1.6 was used. The complete model had a total of about 20.64M cells, with almost 11.19M cells in the impeller, 3.75M in the diffuser, 2.89M in the volute, 2.08M in the ported shroud, and 0.735M in the inlet. The vaned sector model had a total of 2.68M cells, with 1.84M in the impeller, 0.59 in the diffuser, and 0.25 in the inlet. Lastly, the vaneless sector model had a total of 2.82M cells, with 1.85M in the impeller, 0.56M in the diffuser, and 0.41M in the inlet.

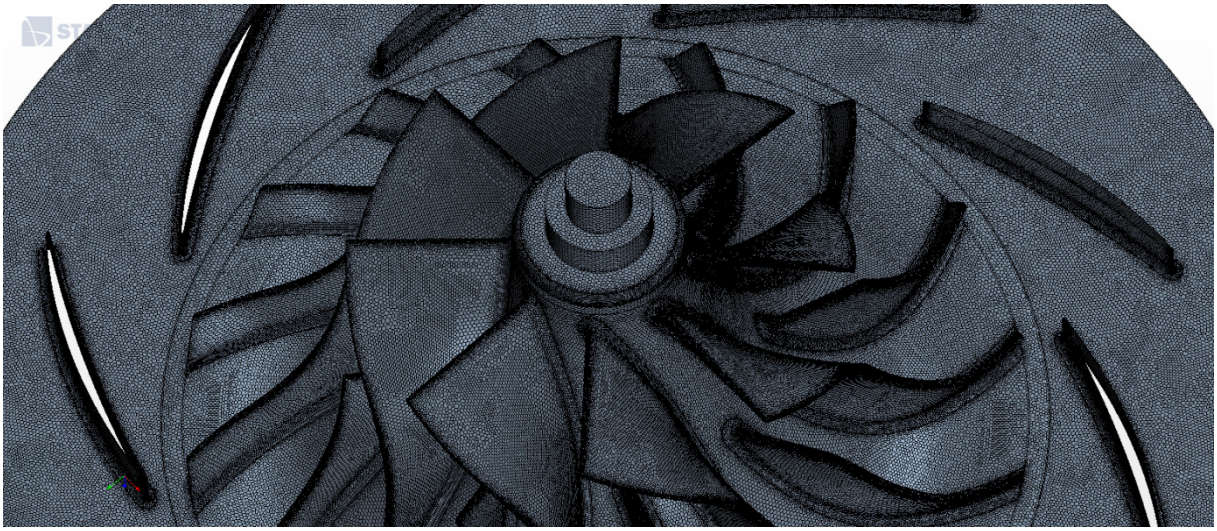

***Figure 4.*** *View of the impeller and diffuser mesh of the complete model of the in-house-compressor.*

Once the mesh was generated the physics models were specified. The physics models define how the selected medium, in this case air, responds to the prevalent conditions. They basically define the primary simulation variables such as pressure, temperature, velocity, and mass, and the mathematical functions used to generate a solution.

The Lag EB (elliptic blending) K-Epsilon turbulence model was used, with a second-order convection scheme, as it was recommended by Siemens for this kind of simulation. Air was selected as the working medium and the ideal gas law was used, where the temperature dependency of the dynamic viscosity and thermal conductivity of the medium was modeled according to Sutherland's Law, while the specific heat ($c_p$) was modeled according to a polynomial.

The rotation of the impeller was modeled with a rotating reference frame in addition to the stationary reference frame. The rotating parts of the impeller were assigned this rotating reference frame.

A coupled solver was used for flow and energy. With the coupled solver, the conservation equations for momentum, energy, species, and continuity are solved simultaneously as a vector of equations. The coupled flow was modeled at second-order discretization with implicit integration.

For the models with a vaned diffuser, the interface between the impeller outlet and diffuser inlet was set to a mixing plane with an implicit connectivity in order to take care of the differences in the tangential velocities, and smooth out any large discrepancies. The same was done for the port interfaces of the ported shroud and impeller for the part load and high load operating points (OP1 and OP3).
The side walls of the sector models were set as interfaces with a periodic topology. The periodic interface connects boundaries that are separated physically by mapping them to each other by some rotation or translation; information is translated across the linked boundaries.

The reference pressure was set to 0.0 Pa so that all pressures would be given in absolute values. The initial conditions were defined with a temperature of 298 K, a turbulence intensity of 5% and viscosity ratio of 100, while the pressure was modified according to each operating point.

#### 2.2.1.3 CFD-Simulation in Star-CCM+

The complete model of the in-house-compressor was simulated in the three previously described operating points. For the design point (OP2) and part load point (OP1), the inlet type was set to "Mass flow inlet", and the outlet type was set to "Pressure outlet". This means that the mass flow at the inlet and the pressure at the outlet were specified according to each operating point, while the pressure at the inlet was dependent on them. When the mass flow and pressure through the compressor in the two simulations had stabilized, the pressure at the outlet was adjusted until the pressure at the inlet reached about 100 kPa. For the high load point, the inlet type was instead set to "Stagnation inlet" with a value of 100 kPa, and the outlet type was kept as a "Pressure outlet". When the flow in the simulation had stabilized, the outlet pressure was adjusted until the mass flow took on a high value close to the operating point and choke region in the map, while still making sure that the flow was not choking.

The vaned sector model was simulated in the same operating points in the same fashion. The mass flow and inlet pressure in all three points was matched as close as possible to that of the complete model. The vaneless sector model was likewise matched to the mass flow and inlet pressure in the two low operating points. For the high load point the mass flow could not be matched before choke occurred. Instead, the total-to-static pressure ratio at the impeller outlet was matched to that of the vaned sector model.

### 2.2.2 Creating the New Design

The new design was created using the design and optimization software in the *TURBOdesign Suite* by *Advanced Design Technology* (ADT). This is a collection of software for aerodynamic 3D design of turbomachinery that enables the user to design, analyze and optimize their choice of turbomachine. Only the design and optimization capabilities within the software package were used in this project. The new design was initially fashioned to match that of the in-house-compressor to assure that it can operate well within similar working conditions, while also constituting a starting point in the design optimization process.

#### 2.2.2.1 TURBOdesign Pre

When designing a new compressor with the *TURBOdesign Suite*, the program TURBOdesign Pre, (TD Pre), is the first one used in the design process.

In TD Pre the mean line design of the impeller and diffuser were generated by stipulating the conditions that make up the chosen design point, along with the desired geometry of each part. Since the new design is meant to act as a replacement, the same design point as that for the in-house-compressor was chosen. The in-house design report was used to assist in this stage.

#### 2.2.2.2 TURBOdesign1

The mean line design of the impeller obtained from TD Pre was imported into TURBOdesign1 (TD1) which is a 3D-geometry generator of the impeller blade and diffuser vane. In TD1 the blade thickness and blade loading distribution, along with various flow parameters, were specified. The grid size of the impeller blade was set to 89 in the streamwise direction and 25 in the spanwise direction, with the multigrid level set to four. Neither blockage factor nor stacking were used for the first draft design. The final design was given a simple linear blockage factor distribution according to values obtained from the CFD-simulations for previous draft designs. The blockage location at the hub and shroud was set to 0.5, the intermediate blockage was set to 0.97 at the hub and 0.95 at the shroud, while the trailing edge blockage was set to 0.94 at the hub and 0.90 at the shroud. The final design was also given a linear stacking distribution with a wrap angle of zero degrees at the hub and five degrees at the shroud, which leads to a so-called rake angle (tangential forward lean) of approximately 40° at the impeller exit. The purpose of this is to reduce the stress level at the blade hub suction surface towards the exit. The gas was set to compressible and ideal while the specifications were unchanged from their TDPre settings. The solver level of the convergence parameters was set to 3D design while the other values were left unchanged. In the initial approach, the design report on the in-house-compressor was used as a guide to achieve similar blade thickness, and the blade loading distribution was specified to give reasonable blade angles and blade surface Mach numbers, while at the same time taking design praxes into account. Once satisfactory results were reached, the first draft design of a new impeller was ready for optimization.

The diffuser was treated similarly, but instead of simply mimicking the thickness distribution of the existing diffuser, a slightly modified NACA-65 profile with 6% thickness was chosen. It is a thickness design that resulted from a combination of another in-house conceptual compressor and the thickness distribution of the diffuser in the in-house-compressor. The grid size was set to 105 in the streamwise direction and 25 in the spanwise direction, with a multigrid level of four. Neither blockage factor nor stacking were used. The gas was set to compressible and ideal, and the convergence parameter was set to 3D design while the other values and specifications were left unchanged. The diffuser was then given a blade loading distribution in the

spanwise direction, $rC_\theta$, in accordance to CFD-results from the in-house-compressor, and a blade loading in the streamwise direction that resulted in decent blade surface Mach numbers. The diffuser design was not run through any optimization.

#### 2.2.2.3 TURBOdesign Optima

The next step in the workflow was to optimize the impeller blade geometry generated in TD1 in TURBOdesign Optima (TD Optima). This is the first of the iterative steps of optimization and CFD-simulations.

TD Optima lets you select a number of input parameters, output constraints, and two output objectives, which are the parameters to be optimized. The input parameters mainly consist of the loading distribution for the main blade and splitter blade, while the output constraints mainly consist of geometrical data and flow- and loss figures. These are each assigned upper and lower limits that they are allowed to fall within. In each calculation in the optimization process, the input parameters and output constraints are combined to generate a solution. If the values of the input and output parameters fall within the stipulated limits, the solution is deemed feasible; a potential blade geometry has been found.

The impeller blade geometry was each time optimized with workflow type 1, in batches of 100 calculations in 120 generations, totaling at 12 000 calculations for each optimization. As input parameters, the blade loading distribution factors for both the full blade and splitter blade were selected and given reasonable variation spans, along with small variations in $rC_\theta$ values for the splitter blades. Various flow- and geometry parameters were selected as output constraints, while combinations of secondary flow factor, leakage loss and profile loss were selected as the optimization objectives. When all the calculations for each optimization are done, the feasible solutions are presented in a plot diagram with the objective parameters at the x- and y-axis.

A couple of solutions were selected and saved as pcf-files (text files) containing the values of the resulting input parameters (blade loading distributions). These were entered and examined in TD1 so that the solution with the best combination of low losses, blade loading, blade surface Mach number, and geometry parameters could be identified.

Once a solution was selected, the leading and trailing edges were modified by assigning them an elliptic shape. The impeller blade geometry was then sent away to be made into a CAD-model for CFD-simulation.

### 2.2.3 Analysis of the New Design

Before a final design was reached, the draft designs were simulated as $1/8^{\text{th}}$ vaneless sector models in order to reduce the simulation time. They were simulated in the same three operating points, with the same mesh-parameters, physics models, and settings as the in-house-compressor. These sector models had a mesh of about 2.63M cells, with 0.55M in the diffuser, 1.65M in the impeller, and 0.42M in the inlet.

Once the simulation of a design was done, new rounds of optimizations were carried out in TD Optima in accordance to the simulation results. A couple of the new optimization results were once more selected to be analyzed in TD1, from among which the next design was picked and again made into a CAD-model, followed by new CFD-simulations. This cycle repeated as many times as the time allowed.
The final design was ultimately complemented with the new diffuser design and simulated as a complete model with ported shroud and volute. The mesh of the complete model of the final design had a total of 27.2M cells, with 0.68 in the inlet, 14.16M in the impeller, 5.59M in the ported shroud, 4.56M in the diffuser, and 2.20M in the volute.

# Chapter 3

# Theory

*The basic physical laws that govern turbomachines will be covered in this chapter. The main focus will be on the centrifugal compressor and its components since those are subject to the design update. The overall function and workings off the turbocharger will be explained briefly.*

## 3.1 Turbochargers

### 3.1.1 How They Work

A turbocharger increases an engine's power output and efficiency. It does this by pushing more air into the cylinders than that of what a naturally aspirated engine could manage. More air in the cylinders means that more fuel can be burned each second, thus letting the engine produce more power.

The main components of a turbocharger are the radial turbine and centrifugal compressor. The turbine wheel is driven by the exhaust gas from the cylinders pushing on its blades, causing it to rotate. This rotation drives the compressor that is connected to the turbine by a shaft and bearing system. The compressor sits in the air intake, compresses the air, and pushes it into the cylinders. The compression causes the temperature of the intake air to increase, which lowers the density of the air. The compressed air is therefore cooled in a heat exchanger before it reaches the cylinders.

## 3.2 Compressor Systems

A compressor is a device that increases the pressure of a flowing gas. Compared to a fan or blower, the pressure rise is substantially larger in a compressor. The pressure ratio in a fan gets up to about 1.1, in a blower to about 1.2, while a compressor achieves ratios well above that. A centrifugal single stage compressor for a turbocharger application gets up to about 4, other applications have achieved ratios as high as 12-14, (Lakshminarayana, 1996), while an axial compressor can achieve numbers well above that (~20-50 for turbofan aircraft engines).

There are a number of different compressor types for various applications, divided into two main groups; *positive displacement compressors* and *dynamic compressors*. These two groups use different techniques of increasing the pressure of the medium.

In a positive displacement compressor, the pressure is increased by reducing the volume of the gas, whereas in a dynamic compressor the gas is accelerated, increasing the kinetic energy, which is transformed to static pressure rise as the gas is diffused. The two main types of dynamic compressors are axial flow compressors and radial flow compressors - there also exist a mixed-flow compressor which is a combination of the two, see *Figure 5.*

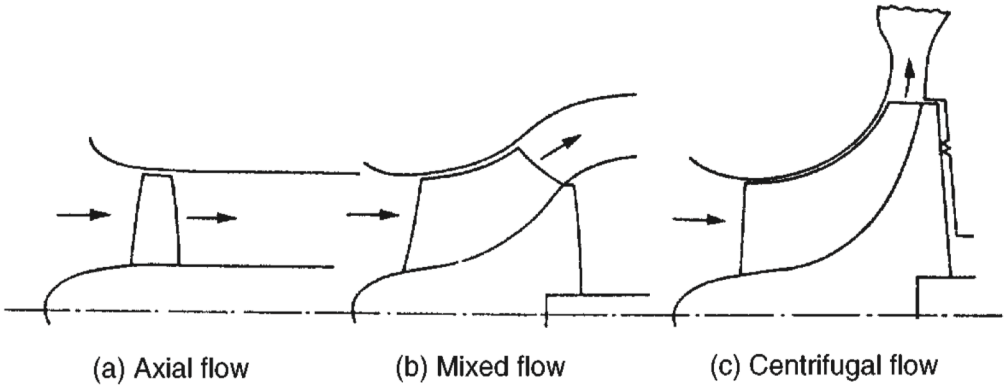


***Figure 5.*** *Different flow types of dynamic compressors (Dixon, 1998).*

In an axial compressor the gas flows through the device along the axial direction. It is made up of a number of stages which each consists of a pair of rotor and stator rows. These rows are in turn made up of a number of blades. The rows of rotor blades rotate with the shaft of the machine and increase the absolute velocity of the gas while decreasing the relative velocity, which increases the static pressure. In turn, the stationary stator blades decrease the absolute velocity of the gas which causes a further increase of static pressure.

In a centrifugal compressor the flow enters axially at a small radius and exits radially at a larger radius. This increase of radius along with the rotation of the machine that give rise to centrifugal and Coriolis forces are the reasons why centrifugal compressors can achieve a much larger pressure ratio in a single stage than that of an axial compressor. However, these drivers also have an adverse effect on the flow through the centrifugal machine in the way of large boundary layers, secondary flows and separation, which is why axial machines have a higher efficiency (Lakshminarayana, 1996). The centrifugal compressor is the type of compressor most commonly used in vehicle turbomachine applications and is described in detail in chapter 4.2.1.

### 3.2.1 Centrifugal Compressor Components

A one-stage centrifugal compressor consists of five distinct parts. These are the inlet, impeller, diffuser, volute, and shroud, which can be ported or not.

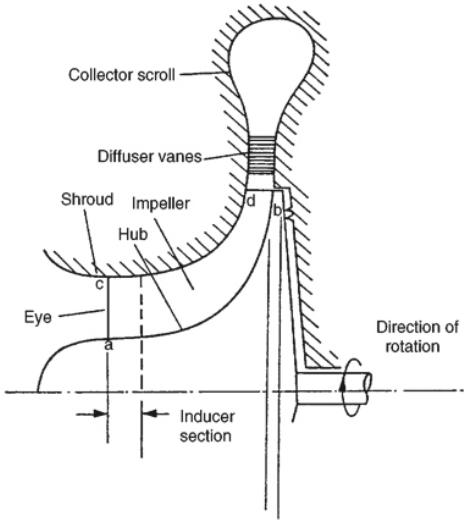


***Figure 6.*** *Cross-section of a centrifugal compressor and its components (Dixon, 1998).*

The inlet is a channel whose purpose it is to bring the incoming flow in a nearly uniform state to the inducer section of the impeller. The inlet may be fitted with inlet guide vanes (IGV's), which are stationary vanes with a variable pitch that can supply a pre-whirl to the flow. This pre-whirl can either be negative or positive, positive being in the direction of impeller rotation.

After the inlet the air reaches the impeller, also called rotor, which is the rotating part of the compressor. As the air flows through the channels of the impeller blades, the flow direction changes from axial at the impeller eye to radial at the trailing edge (location 'd' in *Figure 6*), and the velocity and static pressure of the flow increases due to the centrifugal effect of the larger exit radius and the Coriolis effect that appears due the rotation.

After leaving the impeller the flow travels through the static/stationary diffuser. In the diffuser the flow is decelerated, converting the kinetic energy in the accelerated flow into static pressure. About 50% of the pressure rise takes place in the impeller, and the other 50% in the diffuser. The diffuser can be vaned or vaneless. A vaned diffuser has a smaller operating range and is more expensive compared to a vaneless diffuser but achieves higher pressure ratios due to higher pressure recovery with less losses.

The air finally flows from the diffuser to the volute, (denoted *"collector scroll"* in *Figure 6*). The volutes cross-sectional area gradually increases towards the exit, this causes the flow to decelerate and a further increase of the static pressure takes place.
Some compressors also have a ported shroud. It is a system of ports (or/and channels) that are integrated in the compressor housing (shroud) around the impeller. Its function is to broaden the operational range of the compressor by pushing the surge and choke limits. The phenomena of surge and choke are explained further in chapter 3.5.3, while the workings of the ported shroud are dealt with more in depth in chapter 3.5.3.1.

## 3.3 Thermodynamics

### 3.3.1 Mass and Energy Balance

The first law of thermodynamics states that energy cannot be created or destroyed; it can only change forms, this is also known as *the conservation of energy principle.* Applying the first law to a system undergoing a process the expression can take the form: *"the net change of energy in a system undergoing a process is equal to the difference between the energy entering the system and the energy leaving the system during that process."*

$$E_{in} - E_{out} = \Delta E_{system} \tag{3.1}$$

This can also be expressed in the rate form:

$$\dot{E}_{in} - \dot{E}_{out} = \frac{dE_{system}}{dt} \tag{3.2}$$

Similarly, *the conservation of mass principle* tells us that *"The net mass transfer to or from a control volume during a time interval $\Delta t$ is equal to the net change (increase or decrease) of the total mass within the control volume during $\Delta t$."* (Boles & Çengel, 2015).

$$\sum m_{in} - \sum m_{out} = \Delta m_{CV} \tag{3.3}$$

This can also be expressed in the rate form:

$$\sum \dot{m}_{in} - \sum \dot{m}_{out} = \frac{dm_{CV}}{dt} \tag{3.4}$$

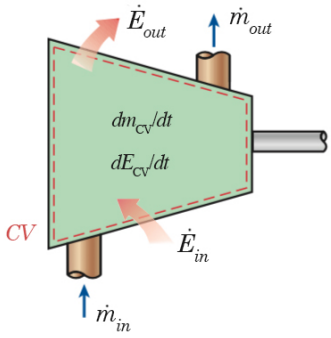


***Figure 7.*** *Arbitrary compressor control volume with mass and energy transfer. Adapted from* (Boles & Çengel, 2015).

A compressor is a device that operates under a steady-flow process. As such, there is no net change of the mass or energy content within the control volume (Boles & Çengel, 2015). For a steady-flow process, the mass and energy balance equations (3.2) and (3.4) reduces to

$$\sum \dot{m}_{in} - \sum \dot{m}_{out} = 0 \quad \rightarrow \quad \sum \dot{m}_{in} = \sum \dot{m}_{out} \tag{3.5}$$

$$\dot{E}_{in} - \dot{E}_{out} = 0 \quad \rightarrow \quad \dot{E}_{in} = \dot{E}_{out} \tag{3.6}$$

Furthermore, a compressor has only one inlet and one outlet, this is referred to as a single-stream process. Denoting the inlet as station 1 and the outlet as station 2, then for steady-flow singe-stream processes the mass balance equation (3.5) reduces to

$$\dot{m}_1 = \dot{m}_2 = \dot{m} \tag{3.7}$$

Equation (3.5) and (3.6) state that the flow rate of mass and energy at the inlet off the control volume is equal to the flow rate of mass and energy at the outlet of the control volume.

Energy can be transported by way of heat, work, and mass (Boles & Çengel, 2015). This gives equation (3.6) the following form

$$\left(\dot{Q} + \dot{W} + \dot{m} \cdot \theta\right)_{in} = \left(\dot{Q} + \dot{W} + \dot{m} \cdot \theta\right)_{out} \tag{3.8}$$

Where $\theta = h + \frac{1}{2}v^2 + gz$ represents flow energy and is made up of specific enthalpy ($h$), kinetic energy ($\frac{1}{2}v^2$), and potential energy ($gz$). The first two terms define the stagnation enthalpy, $h_0 = h + \frac{1}{2}v^2$, while the change in potential energy is negligible and assumed to be $\Delta gz = 0$ (Dixon, 1998). In the case of a compressor which is a work absorbing machine with a (nearly) adiabatic flow process, the following assertions can also be made $\dot{Q}_{in} = \dot{Q}_{out} = \dot{W}_{out} = 0$. These assumptions along with equation (3.7) transform equation (3.8) into

$$\dot{W}_{in} = \dot{W}_c = \dot{m}(h_{02} - h_{01}) \tag{3.9}$$

which represents the total work the compressor exerts on the flowing medium; the power input and is equivalent to the rise in stagnation enthalpy.

### 3.3.2 Specific heat, Ideal gas and Enthalpy

The property that governs "*the energy required to raise the temperature of a unit mass of a substance by one degree"* is called specific heat (Boles & Çengel, 2015). There is specific heat at constant volume, $c_v$, and specific heat at constant pressure, $c_p$.
The energy required for a constant volume process is equal to the change in internal energy, which in turn must be equal to $c_v dT$:

$$\delta e_{in} - \delta e_{out} = du \rightarrow c_v dT = du \rightarrow c_v = \left(\frac{\delta u}{\delta T}\right)_v$$

A corresponding expression for the specific heat for a constant pressure process is obtained in the same manner, where the required energy is equal to the change in enthalpy:

$$\delta e_{in} - \delta e = dh \rightarrow c_h = \left(\frac{\delta h}{\delta T}\right)_h$$

The ratio between the specific heats is defined as $\kappa = \frac{c_p}{c_v}$ and is simply called the specific heat ratio.
The equation of state for an ideal gas can be expressed as

$$pv = RT$$

Joules proved that the internal energy of a gas that can be modeled after the ideal gas law (equation of state) is not dependent on the pressure or specific volume but is solely a function of the temperature (Boles & Çengel, 2015). Combining this knowledge with the equation of state and the definition of enthalpy as follows:

$$\left.\begin{matrix} pv = RT \\ h = u + pv \end{matrix}\right\} h = u + RT$$

one can reason that for an ideal gas enthalpy is also a function of the temperature alone, since R is a constant; $h = h(t)$. Then, from the expressions of specific heats it becomes clear that they are also a function of temperature alone

$$du = c_v(T)dT$$
$$dh = c_p(T)dT$$

The expressions for the change in internal energy and enthalpy for a process working between state 1 and state 2 are obtained by integrating these equations

$$\Delta u = u_2 - u_1 = c_{v,avg}(T_2 - T_1)$$
$$\Delta h = h_2 - h_1 = c_{p,avg}(T_2 - T_1)$$

Where $c_{v,avg}$ and $c_{p,avg}$ are a function of the average temperature of $T_1$ and $T_2$.

## 3.4 Fluid mechanics

### 3.4.1 Newton's Second Law of Motion

Newton's second law of motion states that the time rate of change of a systems momentum relates directly to the net force acting on it. If the acting forces are not

balanced, meaning that the net force is greater than zero, the object will accelerate in the direction of the resulting force.

$$\sum \vec{F}_x = \frac{d}{dt}(\vec{p}) = \frac{d}{dt}\left(m\vec{C}_x\right) = m\vec{a}_x \tag{3.10}$$

Here $\vec{p}$ is the momentum of the object and x is an arbitrary direction. This is known as the momentum equation.

In the case of a compressor which operates under a steady-flow single-stream process, with a control volume according to *Figure 7*, the momentum equation takes the form

$$\sum \vec{F}_x = \dot{m}\left(\vec{C}_{x2} - \vec{C}_{x1}\right) \tag{3.11}$$

where $C_{x2}$ is the steady flow velocity exiting the CV and $C_{x1}$ is the steady flow velocity entering the CV.

### 3.4.2 Moment of Momentum

Since the function of the impeller is to increase the angular momentum of the medium, it is more central to the analysis of compressors to examine Newton's second law as it pertains to the moments of forces.

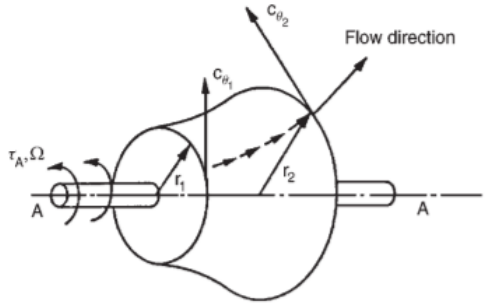


***Figure 8.*** *Control volume and vectors for a general turbomachine (Dixon, 1998).*

The time rate of change of angular momentum of a system with some arbitrary axis of rotation A-A is equal to the torque of the external forces acting on the system.

$$\tau_A = m\frac{d}{dt}(rC_\theta) \tag{3.12}$$

This is the angular momentum equation, or moment of momentum equation. The radius of rotation $r$ is perpendicular to the rotational axis and measures the distance from it to the mass center, while the tangential velocity component $C_\theta$ is perpendicular to both of these. Assigning a control volume around the impeller of a compressor according to *Figure 8*, where the flow enters at radius $r_1$ with the steady tangential flow velocity of $C_{\theta 1}$ and exits at radius $r_2$ with the steady tangential flow velocity $C_{\theta 2}$, the angular momentum equation takes the following form

$$\tau_A = \dot{m}(r_2 C_{\theta 2} - r_1 C_{\theta 1}) \tag{3.13}$$

#### 3.4.2.1 The Euler Pump Equation

The relationship between torque and specific work is defined by

$$\Delta W_c = \frac{\dot{W}}{\dot{m}} = \frac{\tau_A \Omega}{\dot{m}} > 0 \tag{3.14}$$

where $\Omega$ is the angular velocity. Inserting equation (3.9) for power input and equation (3.13) for angular momentum into this relationship, while recognizing that $\Omega r = U$, results in equation (3.15).

$$\Delta W_c = h_{02} - h_{01} = U_2 C_{\theta 2} - U_1 C_{\theta 1} > 0 \tag{3.15}$$

This is known as *Euler's pump equation*, it describes the specific work done on the medium, and it relates the pressure rise across the compressor to the rotational speed. Consulting the velocity triangles at the inlet and outlet of an impeller, (*Figure 9*), and applying the cosine-theorem to express the relative velocities as

$$W_1^2 = C_1^2 + U_1^2 - 2U_1 C_{\theta 1} \tag{3.16}$$

$$W_2^2 = C_2^2 + U_2^2 - 2U_2 C_{\theta 2} \tag{3.17}$$

The Euler pump equation can then be written as

$$\Delta W_c = \frac{1}{2}[(C_2^2 - C_1^2) + (W_1^2 - W_2^2) + (U_2^2 - U_1^2)] \tag{3.18}$$

## 3.5 Compressor Performance

### 3.5.1 Work

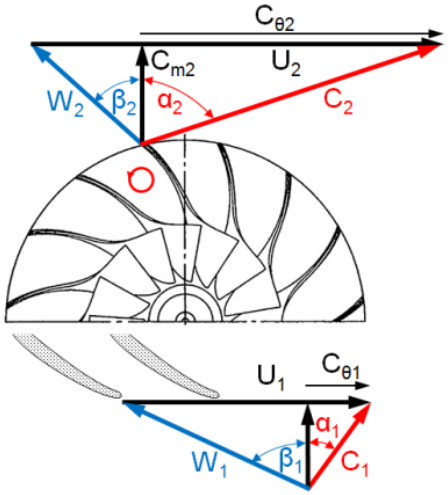


***Figure 9.*** *Velocity triangles at the inlet (1) and outlet (2) of the impeller.*

As mentioned previously in this chapter, the inlet of the compressor may be fitted with inlet guide vanes (IGV's). The compressors work requirement can both increase and decrease with the use of IGV's since the incidence angle from the pre-whirl introduces a tangential absolute velocity component at the inlet, $C_{\theta 1} \neq 0$. The work required to produce the same discharge conditions as without IGV's will decrease in the presence of positive pre-whirl; the impeller doesn't have to do all the work to spin the medium since the air enters the stage with a pre-rotation. A negative pre-whirl with a flow direction opposite the impeller rotation will consequently require more work in order to overcome the opposing flow. The IGV's effect on work requirement becomes evident if one studies Euler's pump equation, equation (3.15) and *Figure 9*, where the flow approaches the eye of the impeller with an angle $\alpha_1 > 0$ (positive pre-whirl). With no IGV's however, $C_{\theta 1} = 0$ and equation (3.15) reduces to

$$\Delta W_c = U_2 C_{\theta 2} > 0 \tag{3.19}$$

### 3.5.2 Efficiencies

For a flow process that goes through a state of change trough compression, the efficiency is defined as the ratio between the ideal change in energy and the actual change in energy. Since a compressor is a work absorbing machine, the ideal change in energy is the smallest possible. Two kinds of efficiencies will be the focus of this chapter. Which one you're talking about depends on which process is denoted as the ideal process. These are the isentropic and polytropic processes and corresponding efficiencies.

#### 3.5.2.1 Isentropic Efficiency

For the isentropic efficiency, the ideal process is the isentropic process, which is adiabatic and internally reversible, where the entropy remains constant, $s_1 = s_2$.

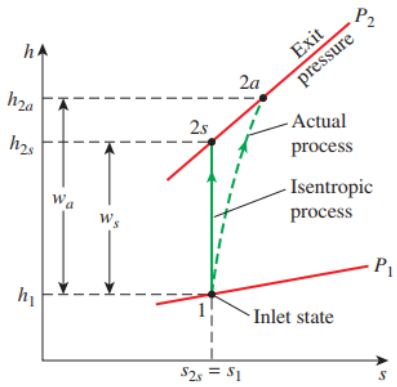


***Figure 10.*** *h-s diagram of the isentropic (solid) and the actual (dashed) compression process* (Boles & Çengel, 2015).

The isentropic efficiency of a compressor is defined as the isentropic enthalpy rise over the impeller divided by the actual enthalpy rise. This is also called the total-to-total isentropic efficiency (indexed by "tt") since it describes the ratio between the change in the total energies, denoted by the subscript 0.

$$\eta_{tt} = \frac{isentropic\ enthalpy\ change}{actual\ enthalpy\ change} = \frac{h_{02,s} - h_{01}}{h_{02} - h_{01}}$$

where $s$ denotes the isentropic state. Applying the relationship between enthalpy and temperature derived in chapter 3.3.2, the total-to-total isentropic efficiency can be expressed as

$$\eta_{tt} = \frac{T_{02,s} - T_{01}}{T_{02} - T_{01}} \tag{3.20}$$

The isentropic relation between the stagnation pressure ratio and stagnation temperature ratio for ideal gases in a compression process are defined by

$$\left(\frac{p_{02}}{p_{01}}\right)^{\left(\frac{\kappa-1}{\kappa}\right)} = \left(\frac{T_{02,s}}{T_{01}}\right) \tag{3.21}$$

Solving this expression for $T_{02,s}$ and inserting that into equation (3.20) results in

$$T_{02,s} = T_{01}\left(\frac{p_{02}}{p_{01}}\right)^{\left(\frac{\kappa-1}{\kappa}\right)} \rightarrow$$
$$\eta_{tt} = \frac{T_{01}}{T_{02} - T_{01}}\left(\left(\frac{p_{02}}{p_{01}}\right)^{\left(\frac{\kappa-1}{\kappa}\right)} - 1\right) \tag{3.22}$$

The isentropic efficiency between the total-to-static states could be of interest for a process where the kinetic energy at the exit isn't used, for example the kinetic energy

at the exit of a volute. The total-to-static isentropic efficiency is denoted "ts" and is likewise formulated

$$\eta_{ts} = \frac{h_{2,s} - h_{01}}{h_{02} - h_{01}} \rightarrow \eta_{ts} = \frac{T_{01}}{T_{02} - T_{01}} \left( \left( \frac{p_2}{p_{01}} \right)^{\left( \frac{\kappa - 1}{\kappa} \right)} - 1 \right)$$

For turbocharger applications however, the total-to-total efficiency is of more interest due to the downstream conditions of the compressor. The flow will reach the charge air cooler after it leaves the compressor volute. If the kinetic energies are high, there will be a lot of pressure losses in the pipes on the way there, along with excessive dumping losses once it reaches the cooler.

### 3.5.2.2 Polytropic Efficiency

The second efficiency is the polytropic efficiency where the polytropic process is deemed the ideal process. The polytropic process can be visualized as a series of very small isentropic processes that follow the actual compression process as illustrated in *Figure 11*.

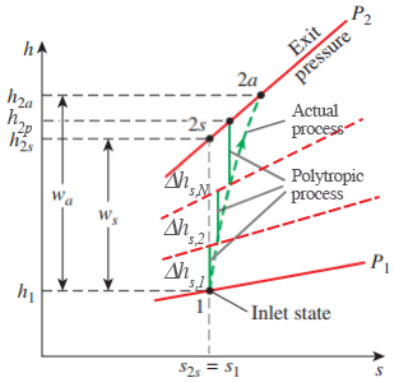


***Figure 11.*** *h-s diagram of the polytropic (solid) and the actual (dashed) compression process. Adapted from* (Boles & Çengel, 2015).

The definition of the polytropic efficiency is thus the ratio between the ideal energy change for a small change in pressure and the actual energy change for that same pressure change. The polytropic relationship between the stagnation pressure ratio and stagnation temperature ratio for ideal gases in a compression process are defined by

$$\left( \frac{p_{02}}{p_{01}} \right)^{\left( \frac{n-1}{n} \right)} = \left( \frac{T_{02}}{T_{01}} \right) \tag{3.23}$$

For a compression process, the polytropic exponent $n$ is related to the isentropic exponent $\kappa$ through

$$\frac{n-1}{n} = \frac{1}{\eta_p}\frac{\kappa-1}{\kappa} \tag{3.24}$$

Combining equation (3.23), (3.24) and (3.21) into equation (3.20) yields the relationship between the isentropic efficiency and the polytropic efficiency

$$\eta_{tt} = \left[\left(\frac{p_2}{p_1}\right)^{\left(\frac{\kappa-1}{\kappa}\right)} - 1\right] \Bigg/ \left[\left(\frac{p_2}{p_1}\right)^{\frac{1}{\eta_p}\left(\frac{\kappa-1}{\kappa}\right)} - 1\right] \tag{3.25}$$

An expression for the polytropic efficiency can be derived from this relationship

$$\eta_p = \frac{\left(\frac{\kappa-1}{\kappa}\right)\log\left(\frac{p_2}{p_1}\right)}{\log\left[\left(\left(\frac{p_2}{p_1}\right)^{\left(\frac{\kappa-1}{\kappa}\right)} - 1\right)\frac{1}{\eta_{tt}} + 1\right]} \tag{3.26}$$

### 3.5.3 Stall, Surge and Choke

In order to understand the phenomena of stall, surge, and choke, one should become familiar with the compressor map and the information it contains. A compressor map is a graph that shows the performance of the compressor within its operational range. The x-axis contains some form of mass flow of the working medium, usually corrected mass flow, while the y-axis contains the discharge pressure, or more commonly the pressure ratio. The map itself consists of constant speed lines for the compressor, also referred to as characteristic lines, ISO lines for compressor efficiency, efficiency islands, surge line, and choke region. The borders or limits of the operational range of the compressor is made up of the lowest and highest speed lines, the surge line on the left, and the choke region to the right. An example of a compressor map can be seen in *Figure 3. Compressor map with the three selected operating points marked in yellow.* Consulting this compressor map, one can see that along the constant speed lines the flow rate is a function of the pressure ratio – as the pressure ratio increases, the flow rate will decrease. Changes in pressure and flow in the compressor are governed by the downstream conditions and arise due to any number of things, one possible reason being a change in the engine's gas demand. It is this relationship between pressure ratio and flow rate, along with the geometrical configuration of the flow passages that enable stall, surge, and choke.

Stall is a local disruption of the uniform flow through the compressor. Stall arises as the pressure increases and the flow rate decreases past a certain point along each speed line in the compressor map. At this point, the retarded flow is no longer able to follow the surface of the impeller, and the flow along the wall reverses. Oncoming streamlines get deflected due to the opposing pressure gradient and viscous shear stresses, and the flow starts to separate from the surface (Japikse, 1996). This

separation most commonly occurs on the suction side of the impeller blade(s) (but can also occur on the pressure side, what's known as negative stall), starting at the trailing edge where the pressure is the highest, and will grow in the direction of the leading edge if the pressure continues to rise. Stall can be isolated to just one blade or affect a couple of blades; it can also jump from blade-passage to blade-passage, rotating around the impeller of the compressor, what's known as rotating stall.

From the compressor map it is evident that the increase in pressure ratio is limited. Physically, this limitation is reached when the forward flow rate is so low that the impeller is no longer able to impart work on the gas – the impeller losses its grip on the gas (Livingston, 2000). The pressure ratio cannot increase past this point, which for a given constant rotational speed is called the surge point – when this point is reached, the compressor experiences surge. The surge line contains all the surge points within the speed range of the compressor. Where stall is a local disruption in the flow, surge is a global, or total, flow disruption. In a compressor that experiences surge the flow direction can momentarily be reversed until the buildup in pressure is reduced to a level at which the impeller is again able to propel the medium. This level is the pressure level that the impeller produces by centrifugal force alone. If the downstream conditions that facilitated the surge to occur in the first place still prevail, this cycle of surge will repeat again; pressure rise until the surge point is reached, flow reduction with possible flow reversal, pressure drop followed by pick up of forward flow. This surge cycling happens on intervals of about one second and is detrimental to the solidity of the compressor, (Livingston, 2000). Temperatures can reach levels above maximum limits, and bearings can get damaged from the resulting vibrations from the changes in flow.

In contrast to stall and surge, choke arise when the compressor operates at a low-pressure ratio and a high flow rate. Although not a clearly defined line like that of the surge line, the choke region defines the operating conditions that will cause the compressor to choke. This region marks the limit of maximum flow rate that the compressor can sustain for each constant speed – further decrease in downstream pressure will not result in a higher flow rate. The flow will in fact get considerably restricted due to blockage effects that arise owing to the high flow conditions. These blockage effects consist of sonic shocks, flow separation, wake regions, and secondary flows within the flow passages of the compressor (Kurz, et al., 2016). In a centrifugal compressor, the throat areas of the impeller and vaned diffuser make up the flow passages that can be affected by choke. Vaneless diffusers rarely affect choke. For high speeds the impeller is the limiting factor and component that will be affected by choke, while for low speeds it is the vaned diffuser. Choke will occur when the sonic flow area and effective throat area are the same. The effective throat area is defined by $A_{th,eff} = C_r A_{th}$ where $C_r$ denotes the throat contraction area caused by viscous area blockage in the throat. The sonic throat area is defined by $A^* = \frac{\dot{m}}{\rho^* C^*}$ (Aungier, 2000). Operation within the choke region is characterized by a considerable drop in pressure rise and efficiency.

#### 3.5.3.1 Methods to Increase Flow Range

One method to reduce the risks of surge and choke where briefly mentioned in chapter 4.2.1, this and a few more will be further explained in this chapter. The ambition is to have a machine with a wide operational range that is able to handle a slew of changeable conditions. The upper limit of the flow rate is defined by the choke mass flow of the impeller or diffuser and is directly dependent on their respective throat area. The lower limit of the flow rate is defined by the surge mass flow, which depends on the current pressure, velocity, rotational speed and density conditions. The geometry of the impeller blade also plays a role.

The use of a ported shroud has the biggest impact on range extension, pushing the limit of both the surge and choke mass flow. If the operation of the compressor approaches the surge line, the ported shroud will re-circulate some of the flow in the impeller back to its inlet, increasing the flow rate, thereby moving away from the surge line in the compressor map. If the operation is instead approaching the choke region, the ported shroud will allow a diversion of some of the flow, bypassing the impeller throat, and reducing the risk of choking while maintaining a high flow rate.

Reducing the number of blades in the impeller and using splitter blades will increase the throat area and reduce the risk of choking.

The pre-whirl produced by inlet guide vanes (IGV's) will not only affect the work requirement of the compressor, it will also influence the relative flow velocity at the impeller inlet. A positive pre-whirl will reduce the relative velocity, while a negative pre-whirl will increase it. Positive pre-whirl will reduce the loading of the inlet; the incidence angle becomes smaller at low flows, and the surge line is moved towards lower flow regimes (to the left in the compressor map). The use of pre-whirl is therefore used for operation at low flows. A slightly negative pre-whirl will allow for a small increase of the flow rate at high rpm's due to a better interplay between the incidence angle and the blade at those kinds of operating conditions (Ising, 2017). This effectively broadens the operating range of the compressor.

A vaneless diffuser is a way to accommodate high flow rates though the diffuser. Without vanes the problem of a restricting throat area is done away with.

### 3.5.4 Losses

#### 3.5.4.1 Slip

Slip is a deviation in the angle of the relative flow from the actual blade angle at the impeller tip/exit. Slip results in a reduced tangential absolute velocity at the outlet, $C_{\theta 2}$, which consequently affects the work output of the machine negatively.
Slip arises due to what's called the relative eddy. In a flow regime where the absolute flow enters and leaves the impeller without whirl, the relative flow rotates within the impeller passage in the reverse direction to the impeller rotation; this is termed the

relative eddy. If the angular velocity of the impeller is Ω, the angular velocity of the relative eddy is –Ω (Dixon, 1998).
The relative flow at the outlet of the impeller can be viewed as a through-flow with a relative eddy superimposed on it. The combined effect of these two flow-types results in a relative flow at the impeller outlet with the angle $\beta_2$ which is not equal to the blade angle $\beta'_2$, and a flow direction opposite to the impeller rotation.
The slip factor is symbolized by "$\sigma$" and defined as the ratio between the actual tangential absolute velocity and the ideal tangential absolute velocity at the impeller outlet (Dixon, 1998). A value of unity signifies no slip.

$$\sigma = \frac{C_{\theta 2}}{C'_{\theta 2}} < 1$$

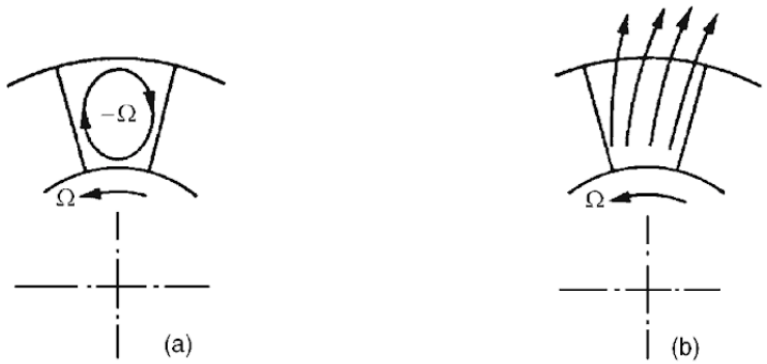


***Figure 12.*** *(a) The relative eddy without through-flow, (b) the relative flow at the impeller outlet that is the product of both through-flow and relative eddy (Dixon, 1998).*

For radial blades where $\beta_2 = 0$ the ideal tangential absolute velocity component is equal to the tip speed of the blade, $C'_{\theta 2} = U_2$. A higher number of blades will reduce the slip in the flow since they will be able to guide the flow better but would also reduce the effective flow area (Cohen, et al., 1996).

#### 3.5.4.2 Friction

The friction losses are various. In the vaneless diffuser there is a lot of skin friction resulting from the long path of the unguided flow. The vaned diffuser also suffers from skin friction within the vane channels, but less so due to the shorter length of travel. The angle of divergence will also affect the friction losses in the diffuser, since a small angle would suggest a long diffuser and more skin friction (Cohen, et al., 1996).
High absolute Mach numbers into the diffuser, $M_2$, will also lead to high friction losses due to inefficiencies in the diffusion under such flow regimes.
Shrouded impellers have the benefit of no tip leakage losses, but as a consequence suffer an increase of friction losses.
An impeller with a high number of blades and the same mass flow as that of an impeller with a lower number of blades will suffer more friction losses due to the fact

that the inlet velocity must be increased to compensate for the loss in effective flow area (Cohen, et al., 1996).

#### 3.5.4.3 Tip Leakage

The importance of tip clearance was briefly touched upon in chapter 2. The tip clearance is always important to consider for un-shrouded impellers since it will cause tip leakage. Tip leakage is when the air flows from the high-pressure side of a blade-passage, over the tip of the blade to the lower pressure side of the adjacent blade-passage. This leakage has a direct effect on the stage efficiency; Japikse writes that as a rule, one point of stage efficiency is lost for every 3% of the passage exit height that is added to the tip clearance (Japikse, 1996).

## 3.6 Centrifugal Compressor Design

### 3.6.1 The Design Process

There are many different ways to approach the design of a turbomachine. Japikse describes the process as consisting of three different levels. At the first level, the new design is obtained through similitude by scaling other already existing designs. This is an easy, cost effective way to go about procuring a family of machines with similar geometry for different applications. At the second level, one moves away from solely looking at the performance of the single component (i.e. an impeller), to also incorporate how neighboring components (i.e. diffuser) perform under different design conditions in order to best match these together. At the third level, the use of models is incorporated in the design regime of each element of the machine. Such models could be (but are not limited to) the effects from core flow, boundary layers, secondary flow, and mixing processes, occurring throughout the machine (Japikse, 1996).
Another thing that Japikse and other authors mention is the experience that each designer brings to his or her work. It is something that permeates all of the aforementioned levels, and it means that there are probably as many approaches to design as there are designers.

### 3.6.2 Common Design Features

#### 3.6.2.1 Inlet Options

**Inlet guide vanes (IGV)** – The impact of the use of IGV's on the compressor operation have been covered previously. They include a wider flow range and some control on the required work input.

### 3.6.2.2 Impeller Options

**Backward-swept blades** – the use of back-swept blades at the trailing edge of the impeller will reduce the tangential component of the absolute velocity, which will reduce the work absorbing capacity of the impeller. It will on the other hand achieve higher pressure ratios at low flows, as well as more range and more stable operation than that of an impeller with radial blades. Back-swept blades will also result in a machine with higher efficiency for the same power produced. If the axial velocity and power is the same between a machine with radial blades and one with back-swept blades, then $U_2 C_{\theta 2}$ must also be the same between the two. $C_{\theta 2}$ in the back-swept compressor is lower, meaning that $U_2$ must be higher, either by a greater rpm or a larger impeller exit diameter. In addition, the absolute velocity $C_2$ leaving the impeller will also be lower, which can be seen to the right in *Figure 13*, this means that the kinetic energy entering the diffuser is lower. This leads to lower diffuser losses and a higher efficiency. As a drawback, the higher $U_2$ results in higher stresses (Japikse, 1996). Typical angles of back-sweep range between -30° to -50° from the radial position.

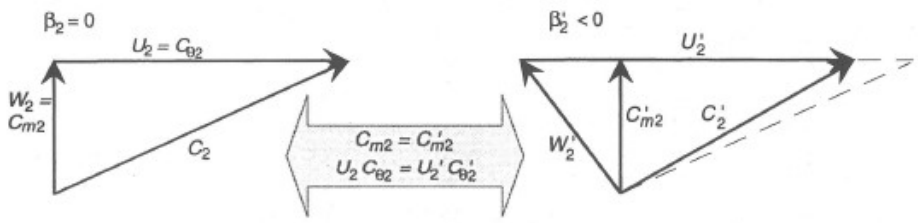


***Figure 13.*** *Velocity triangles for radial blades (left) and back-swept blades (right)* (Japikse, 1996).

### 3.6.2.3 Diffuser Options

**Vaneless diffuser** – Vaneless diffusers are used for compressors that need to be able to operate under a wide flow range. The absence of vane passages means little to no demand on the angle of the flow leaving the impeller. The consequence being that flow with high swirl will travel a long way before leaving the diffuser, which is accompanied with a lot of wall rubbing and friction losses. Additionally, the vaneless design lacks the vibratory coupling between the impeller and diffuser vanes that can result in fatigue failure. A vaneless diffuser is cheaper to manufacture than a vaned one (Japikse, 1996).

**Vaned diffuser** – The vaned diffuser places a higher demand on the flow. A low flow rate will lead to high diffusion which results in separation and can lead to surge. A high flow rate will lead to acceleration through the vane passages which means high Mach numbers that can lead to choke. On the other hand, the vaned diffuser has a higher efficiency and can achieve higher pressure ratios than its vaneless counterpart.

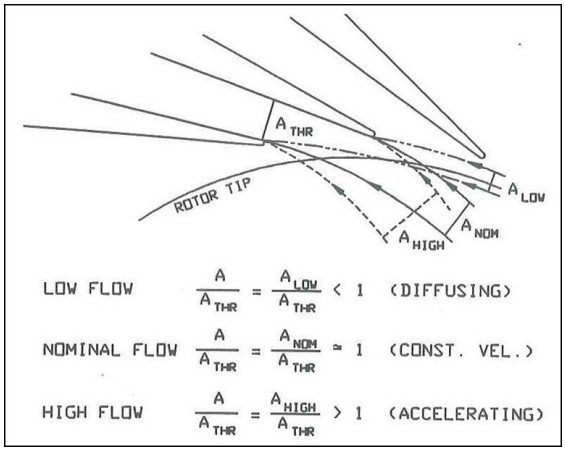


***Figure 14.*** *Different flow regimes at the throat of a diffuser flow passage* (Japikse, 1996).

#### 3.6.2.4 Design Guidelines

Owing to the existence of common praxes in centrifugal compressor design, one doesn't have to "re-invent the wheel" each time. These praxes are a set of guidelines with (often) favorable effects on the compressor performance. A couple of these are presented below.

- The ratio between the tip radius of the leading edge and the radius of the impeller outlet, $\frac{r_{1,tip}}{r_2}$, should at least be between 0.5 and 0.8. The lower limit results in a long channel with losses, while the upper limit will produce a poor meridional profile. It is best to keep between 0.6 and 0.65.

- The ratio between the trailing edge blade height and the impeller exit radius, $\frac{b_2}{r_2}$, will ideally fall between 0.05 and 0.15 (Korpela, 2011). Values below the lower limit will form a channel that is too narrow, while values above the upper limit will result in too high diffusion.

- The ratio between the leading-edge hub radius and leading-edge tip radius, $\frac{r_{1,hub}}{r_{1,tip}}$, is usually between 0.3 and 0.7, where the lower limit is restricted by disturbances such as vibrations and high relative Mach numbers, while the upper limit is set to attain a sufficient blade height and throat area to allow for decent flow rates. It is a ratio used in the optimization (minimization) of the relative tip velocity at the inlet in order to achieve the most efficient stage design (Japikse, 1996).

- The blade tip angle at the impeller leading edge, $\beta_1$, should be above -70° to avoid blockage of the channel by the turning of the blade. A minimized Mach number is obtained from blade angles of around -58°, and it's advised to optimize for this (Korpela, 2011).

- The exit angle of the flow, $\alpha_2$, should fall between 63° and 72° (Korpela, 2011), possibly as high as 80° if the diffuser is vaned, for a vaneless diffuser, exit angles in the higher digits may involve high diffuser losses, due to the large tangential velocity component.

# Chapter 4

# Results

*The results from the work performed as described under chapter 2 is presented in the following chapter. The simulation results for the in-house-compressor are presented first. These results constitute the benchmark for the new design. This is followed by the corresponding simulation results for the new design and its design guideline parameters in accordance to chapter 3.6.2.4. Some figures of the results are also presented to highlight different findings; these are discussed more in detail in chapter* 5 Discussion.

## 4.1 In-House-Compressor

**Table 1.** Collected results from the CFD-simulations of the in-house-compressor. Un-shaded entries are output collected from Star-CCM+. Shaded entries are calculated from the output.

| | | **OP1** | **OP2** | **OP3** |
|---|---|---|---|---|
| Rotational speed | rpm | 71350 | 91765 | 108500 |
| Tip speed | m/s | 380.52 | 489.40 | 578.65 |
| Air mass flow | kg/s | 0.2144 | 0.395 | 0.4854 |
| Total inlet pressure | Pa | 100027 | 99969 | 100000 |
| Total inlet temperature | K | 298 | 298 | 298 |
| **Impeller exit** | | | | |
| Total pressure, mass avg | Pa | 251846 | 371759 | 520860 |
| Total pressure, area avg | Pa | 249810 | 366804 | 513709 |
| Static pressure, area avg | Pa | 184312 | 238249 | 301786 |
| Total temperature | K | 402.06 | 452.30 | 510.55 |
| Mach number, mass avg | | 0.686 | 0.827 | 0.922 |
| Mach number, area avg | | 0.677 | 0.814 | 0.910 |
| Flow angle, area avg | deg | 74.53 | 70.79 | 72.41 |
| Flow angle, mass avg | deg | 71.64 | 65.27 | 65.88 |
| Pressure ratio (t/t), mass avg | | **2.518** | **3.719** | **5.209** |
| Pressure ratio (t/t), area avg | | 2.497 | 3.669 | 5.137 |
| Pressure ratio (t/s), area avg | | 1.843 | 2.383 | 3.018 |
| Isentropic efficiency (t/t), mass avg | | **0.855** | **0.869** | **0.835** |
| Isentropic efficiency (t/t), area avg | | 0.847 | 0.859 | 0.826 |
| Isentropic efficiency (t/s), area avg | | 0.541 | 0.538 | 0.514 |
| Polytropic efficiency (t/t), mass avg | | **0.872** | **0.891** | **0.867** |
| Polytropic efficiency (t/t), area avg | | 0.865 | 0.882 | 0.860 |
| **Diffuser exit** | | | | |
| Total pressure, mass avg | Pa | 239438 | 352970 | 480928 |
| Total pressure, area avg | Pa | 237441 | 348888 | 476585 |
| Static pressure, area avg | Pa | 226993 | 320710 | 439745 |
| Static pressure recovery, $C_p$ | | 0.632 | 0.618 | 0.630 |
| Mach number, mass avg | | 0.278 | 0.374 | 0.361 |

| | | | | |
|---|---|---|---|---|
| Mach number, area avg | | 0.255 | 0.350 | 0.342 |
| Flow angle, area avg | deg | 64.76 | 65.56 | 66.26 |
| Flow angle, mass avg | deg | 63.71 | 63.46 | 64.40 |
| Pressure ratio (t/t), mass avg | | **2.394** | **3.531** | **4.809** |
| Pressure ratio (t/t), area avg | | 2.374 | 3.490 | 4.766 |
| Pressure ratio (t/s), area avg | | 2.269 | 3.208 | 4.397 |
| Isentropic efficiency (t/t), mass avg | | **0.800** | **0.826** | **0.780** |
| Isentropic efficiency (t/t), area avg | | 0.791 | 0.817 | 0.775 |
| Isentropic efficiency (t/s), area avg | | 0.745 | 0.752 | 0.726 |
| Polytropic efficiency (t/t), mass avg | | **0.822** | **0.853** | **0.822** |
| Polytropic efficiency (t/t), area avg | | 0.814 | 0.845 | 0.817 |
| **Volute exit** | | | | |
| Exit diameter, Ø | mm | 50 | 50 | 50 |
| Total pressure, mass avg | Pa | 234319 | 340903 | 465951 |
| Total pressure, area avg | Pa | 234263 | 340766 | 465756 |
| Static pressure, area avg | Pa | 231000 | 332100 | 45000 |
| Total temperature | K | 401.79 | 451.89 | 510.40 |
| Static pressure recovery, $C_p$ | | 0.691 | 0.703 | 0.699 |
| Static pressure recovery, $C_p$, in volute | | 0.322 | 0.3531 | 0.3704 |
| Mach number, mass avg | | 0.144 | 0.195 | 0.186 |
| Mach number, area avg | | 0.143 | 0.194 | 0.184 |
| Pressure ratio (t/t), mass avg | | **2.343** | **3.410** | **4.660** |
| Pressure ratio (t/t), area avg | | 2.342 | 3.409 | 4.658 |
| Pressure ratio (t/s), area avg | | 2.309 | 3.322 | 4.550 |
| Isentropic efficiency (t/t), mass avg | | **0.776** | **0.798** | **0.760** |
| Isentropic efficiency (t/t), area avg | | 0.776 | 0.797 | 0.759 |
| Isentropic efficiency (t/s), area avg | | 0.762 | 0.778 | 0.745 |
| Polytropic efficiency (t/t), mass avg | | **0.801** | **0.828** | **0.804** |
| Polytropic efficiency (t/t), area avg | | 0.801 | 0.828 | 0.804 |
| | | | | |
| Moment | Nm | 3.040 | 6.425 | 9.260 |
| Power | W | 22711 | 61737 | 105215 |
| Efficiency (t/t) | | **0.7767** | **0.8017** | **0.7599** |
| Ported shroud flow | kg/s | -0.0443 | 0.0043 | 0.0153 |

## 4.2 The New Design

**Table 2.** Collected results from the CFD-simulations of the new design. Un-shaded entries are output collected from Star-CCM+. Shaded entries are calculated from the output. Entries with red borders contain the parameter that was matched to the in-house-compressor simulation result for the specific operating point.

| | | **OP1** | **OP2-1** | **OP2-2** | **OP3** |
|---|---|---|---|---|---|
| Rotational speed | rpm | 71600 | 92087 | 92087 | 108881 |
| Tip speed | m/s | 380.52 | 489.40 | 489.40 | 578.65 |
| Air mass flow | kg/s | 0.2144 | 0.3950 | 0.3893 | 0.4732 |
| Total inlet pressure | Pa | 99982 | 100081 | 100000 | 100000 |
| Total inlet temperature | K | 298 | 298 | 298 | 298 |
| **Impeller exit** | | | | | |

| | | | | | |
|---|---|---|---|---|---|
| Total pressure, mass avg | Pa | 248351 | 369177 | 371464 | 524377 |
| Total pressure, area avg | Pa | 246549 | 364621 | 367152 | 513691 |
| Static pressure, area avg | Pa | 183766 | 241541 | 243164 | 310595 |
| Total temperature | K | 397.71 | 446.31 | 447.27 | 503.90 |
| Mach number, mass avg | | 0.673 | 0.806 | 0.806 | 0.902 |
| Mach number, area avg | | 0.665 | 0.794 | 0.794 | 0.883 |
| Flow angle, area avg | deg | 72.83 | 68.84 | 69.28 | 71.40 |
| Flow angle, mass avg | deg | 71.14 | 65.68 | 66.28 | 67.71 |
| Pressure ratio (t/t), mass avg | | **2.484** | **3.689** | **3.715** | **5.244** |
| Pressure ratio (t/t), area avg | | 2.466 | 3.643 | 3.672 | 5.137 |
| Pressure ratio (t/s), area avg | | 1.838 | 2.413 | 2.432 | 3.106 |
| Isentropic efficiency (t/t), mass avg | | **0.878** | **0.898** | **0.898** | **0.866** |
| Isentropic efficiency (t/t), area avg | | 0.870 | 0.888 | 0.888 | 0.852 |
| Isentropic efficiency (t/s), area avg | | 0.562 | 0.569 | 0.571 | 0.547 |
| Polytropic efficiency (t/t), mass avg | | **0.892** | **0.915** | **0.915** | **0.893** |
| Polytropic efficiency (t/t), area avg | | 0.885 | 0.906 | 0.906 | 0.882 |
| **Diffuser exit** | | | | | |
| Total pressure, mass avg | Pa | 235318 | 349172 | 350814 | 477731 |
| Total pressure, area avg | Pa | 234241 | 345742 | 347503 | 474440 |
| Static pressure, area avg | Pa | 224922 | 321383 | 323885 | 445425 |
| Static pressure recovery, $C_p$ | | 0.6372 | 0.6255 | 0.6292 | 0.6307 |
| Mach number, mass avg | | 0.256 | 0.347 | 0.341 | 0.319 |
| Mach number, area avg | | 0.242 | 0.326 | 0.320 | 0.302 |
| Flow angle, area avg | deg | 62.56 | 62.20 | 62.22 | 62.58 |
| Flow angle, mass avg | deg | 61.17 | 60.64 | 60.69 | 61.17 |
| Pressure ratio (t/t), mass avg | | **2.354** | **3.489** | **3.508** | **4.777** |
| Pressure ratio (t/t), area avg | | 2.343 | 3.455 | 3.475 | 4.744 |
| Pressure ratio (t/s), area avg | | 2.250 | 3.211 | 3.239 | 4.454 |
| Isentropic efficiency (t/t), mass avg | | **0.807** | **0.842** | **0.841** | **0.775** |
| Isentropic efficiency (t/t), area avg | | 0.803 | 0.835 | 0.833 | 0.771 |
| Isentropic efficiency (t/s), area avg | | 0.760 | 0.777 | 0.778 | 0.732 |
| Polytropic efficiency (t/t), mass avg | | **0.829** | **0.867** | **0.866** | **0.817** |
| Polytropic efficiency (t/t), area avg | | 0.824 | 0.860 | 0.859 | 0.814 |
| **Volute exit** | | | | | |
| Exit diameter, Ø | mm | 50 | 50 | 50 | 50 |
| Total pressure, mass avg | Pa | 231302 | 338705 | 340622 | 465401 |
| Total pressure, area avg | Pa | 231256 | 338598 | 340519 | 465269 |
| Static pressure, area avg | Pa | 228000 | 330000 | 332203 | 455000 |
| Total temperature | K | 398.55 | 447.13 | 448.23 | 510.70 |
| Static pressure recovery, $C_p$ | | 0.685 | 0.693 | 0.694 | 0.676 |
| Static pressure recovery, $C_p$, in volute | | 0.296 | 0.310 | 0.309 | 0.296 |
| Mach number, mass avg | | 0.145 | 0.195 | 0.191 | 0.181 |
| Mach number, area avg | | 0.144 | 0.194 | 0.190 | 0.180 |
| Pressure ratio (t/t), mass avg | | **2.314** | **3.384** | **3.406** | **4.654** |
| Pressure ratio (t/t), area avg | | 2.313 | 3.383 | 3.405 | 4.653 |
| Pressure ratio (t/s), area avg | | 2.280 | 3.297 | 3.322 | 4.550 |
| Isentropic efficiency (t/t), mass avg | | **0.788** | **0.817** | **0.816** | **0.758** |
| Isentropic efficiency (t/t), area avg | | 0.788 | 0.817 | 0.816 | 0.758 |
| Isentropic efficiency (t/s), area avg | | 0.773 | 0.796 | 0.796 | 0.744 |
| Polytropic efficiency (t/t), mass avg | | **0.811** | **0.845** | **0.844** | **0.803** |
| Polytropic efficiency (t/t), area avg | | 0.811 | 0.845 | 0.844 | 0.802 |

| **Total** | | | | | |
|---|---|---|---|---|---|
| Moment | Nm | 2.924 | 6.216 | 6.168 | 8.896 |
| Power | W | 21928 | 59946 | 59480 | 101429 |
| Efficiency (t/t) | | **0.7912** | **0.8197** | **0.8192** | **0.7677** |
| Ported shroud flow | kg/s | -0.0417 | 0.0003 | 0.0003 | 0.0340 |

### 4.2.1 Design Guidelines

Some of the design guideline parameters from chapter 3.6.2.4 for the new design are presented below:

- $\frac{r_{1,tip}}{r_2} = 0.61$
- $\frac{b_2}{r_2} = 0.089$
- $\frac{r_{1,hub}}{r_{1,tip}} = 0.35$
- $\beta_1 = -62.7°$
- $\alpha_{2,area\ avg} = 68.84°$; $\alpha_{2,mass\ flow\ avg} = 65.68°$

## 4.3 Comparisons

**Table 3.** Efficiency comparisons between the new design and in-house-compressor for the part load point, OP1.

| **OP1** | **New design** | **In-house** | **Difference** |
|---|---|---|---|
| **Impeller exit** | | | |
| Isentropic efficiency (t/t), mass avg | 0.878 | 0.855 | **+2.3 %-points** |
| Isentropic efficiency (t/s), area avg | 0.562 | 0.541 | **+2.1 %-points** |
| Polytropic efficiency (t/t), mass avg | 0.892 | 0.872 | **+2.0 %-points** |
| Average efficiency improvement | | | **+2.13 %-points** |
| **Diffuser exit** | | | |
| Isentropic efficiency (t/t), mass avg | 0.807 | 0.800 | **+0.7 %-points** |
| Isentropic efficiency (t/s), area avg | 0.760 | 0.745 | **+1.5 %-points** |
| Polytropic efficiency (t/t), mass avg | 0.829 | 0.822 | **+0.7 %-points** |
| Average efficiency improvement | | | **+0.97%-points** |
| **Volute exit** | | | |
| Isentropic efficiency (t/t), mass avg | 0.788 | 0.776 | **+1.2 %-points** |
| Isentropic efficiency (t/s), area avg | 0.773 | 0.762 | **+1.1 %-points** |
| Polytropic efficiency (t/t), mass avg | 0.811 | 0.801 | **+1.0 %-points** |
| Average efficiency improvement | | | **+1.10 %-points** |
| **Compressor total** | | | |
| Isentropic efficiency (t/t), mass avg | 0.7912 | 0.7767 | **+1.45 %-points** |

**Table 4.** Efficiency comparisons between the new design and in-house-compressor for the design point where the mass flow rate was matched between the simulations, OP2-1.

| **OP2-1** | **New Design** | **In-house** | **Difference** |
|---|---|---|---|
| **Impeller exit** | | | |
| Isentropic efficiency (t/t), mass avg | 0.898 | 0.869 | **+2.9 %-points** |
| Isentropic efficiency (t/s), area avg | 0.569 | 0.538 | **+3.1 %-points** |
| Polytropic efficiency (t/t), mass avg | 0.915 | 0.891 | **+2.4 %-points** |
| Average efficiency improvement | | | **+2.8 %-points** |
| **Diffuser exit** | | | |
| Isentropic efficiency (t/t), mass avg | 0.842 | 0.826 | **+1.6 %-points** |
| Isentropic efficiency (t/s), area avg | 0.777 | 0.752 | **+2.5 %-points** |
| Polytropic efficiency (t/t), mass avg | 0.867 | 0.853 | **+1.4%-points** |
| Average efficiency improvement | | | **+1.83%-points** |
| **Volute exit** | | | |
| Isentropic efficiency (t/t), mass avg | 0.817 | 0.798 | **+1.9 %-points** |
| Isentropic efficiency (t/s), area avg | 0.796 | 0.778 | **+1.8 %-points** |
| Polytropic efficiency (t/t), mass avg | 0.845 | 0.828 | **+1.7 %-points** |
| Average efficiency improvement | | | **+1.80 %-points** |
| **Compressor total** | | | |
| Isentropic efficiency (t/t), mass avg | 0.8197 | 0.8017 | **+1.8 %-points** |

**Table 5.** Efficiency comparisons between the new design and in-house-compressor for the design point where the total-to-static pressure ratio at the outlet was matched between the simulations, OP2-2.

| **OP2-2** | **New Design** | **In-house** | **Difference** |
|---|---|---|---|
| **Impeller exit** | | | |
| Isentropic efficiency (t/t), mass avg | 0.898 | 0.869 | **+2.9 %-points** |
| Isentropic efficiency (t/s), area avg | 0.571 | 0.538 | **+3.3 %-points** |
| Polytropic efficiency (t/t), mass avg | 0.915 | 0.891 | **+2.4 %-points** |
| Average efficiency improvement | | | **+2.87 %-points** |
| **Diffuser exit** | | | |
| Isentropic efficiency (t/t), mass avg | 0.841 | 0.826 | **+1.5 %-points** |
| Isentropic efficiency (t/s), area avg | 0.778 | 0.752 | **+2.6 %-points** |
| Polytropic efficiency (t/t), mass avg | 0.866 | 0.853 | **+1.3%-points** |
| Average efficiency improvement | | | **+1.80 %-points** |
| **Volute exit** | | | |
| Isentropic efficiency (t/t), mass avg | 0.816 | 0.798 | **+1.8 %-points** |
| Isentropic efficiency (t/s), area avg | 0.796 | 0.778 | **+1.8 %-points** |
| Polytropic efficiency (t/t), mass avg | 0.844 | 0.828 | **+1.6 %-points** |
| Average efficiency improvement | | | **+1.73 %-points** |
| **Compressor total** | | | |
| Isentropic efficiency (t/t), mass avg | 0.8192 | 0.8017 | **+1.75 %-points** |

**Table 6.** Efficiency comparisons between the new design and in-house-compressor for the high load point OP3.

| **OP3** | **New Design** | **In-house** | **Difference** |
|---|---|---|---|
| **Impeller exit** | | | |
| Isentropic efficiency (t/t), mass avg | 0.866 | 0.835 | **+3.1 %-points** |
| Isentropic efficiency (t/s), area avg | 0.547 | 0.514 | **+3.3 %-points** |
| Polytropic efficiency (t/t), mass avg | 0.893 | 0.867 | **+2.6 %-points** |
| Average efficiency improvement | | | **+3.00%-points** |
| **Diffuser exit** | | | |
| Isentropic efficiency (t/t), mass avg | 0.775 | 0.780 | **-0.5 %-points** |
| Isentropic efficiency (t/s), area avg | 0.732 | 0.726 | **+0.6 %-points** |
| Polytropic efficiency (t/t), mass avg | 0.817 | 0.822 | **-0.5 %-points** |
| Average efficiency improvement | | | **-0.13%-points** |
| **Volute exit** | | | |
| Isentropic efficiency (t/t), mass avg | 0.758 | 0.760 | **-0.2 %-points** |
| Isentropic efficiency (t/s), area avg | 0.744 | 0.745 | **-0.1 %-points** |
| Polytropic efficiency (t/t), mass avg | 0.803 | 0.804 | **-0.1 %-points** |
| Average efficiency improvement | | | **-0.13 %-points** |
| **Compressor total** | | | |
| Isentropic efficiency (t/t), mass avg | 0.7677 | 0.7599 | **+0.78 %-points** |

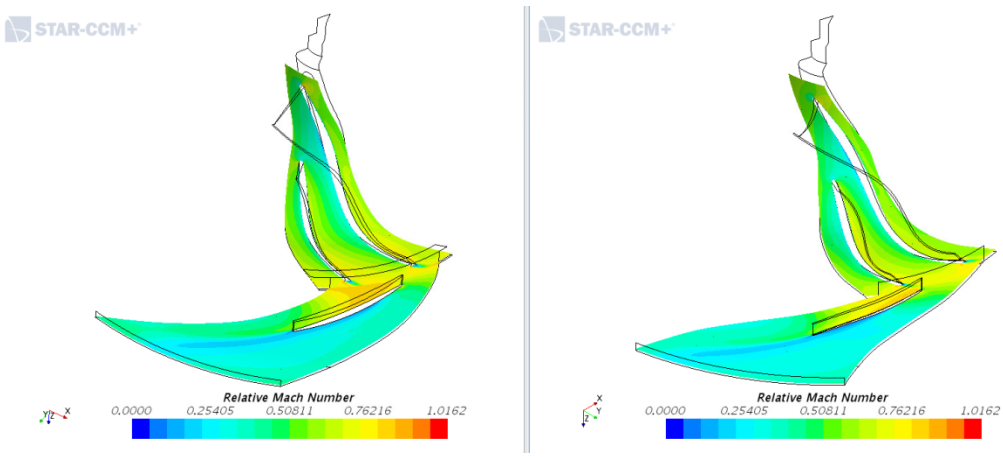


***Figure 15.*** *Sector analysis of the relative Mach number in the impeller and diffuser at 20% spanwise location, simulated in the design point (OP2-1 for the new design). In-house-compressor on the left, new design on the right.*

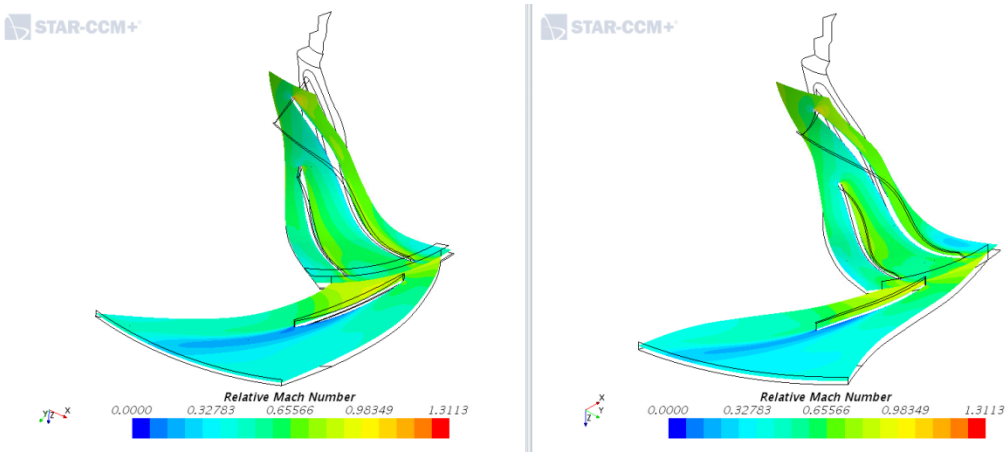


***Figure 16.*** *Sector analysis of the relative Mach number in the impeller and diffuser at 50% spanwise location, simulated in the design point (OP2-1 for the new design). In-house-compressor on the left, new design on the right.*

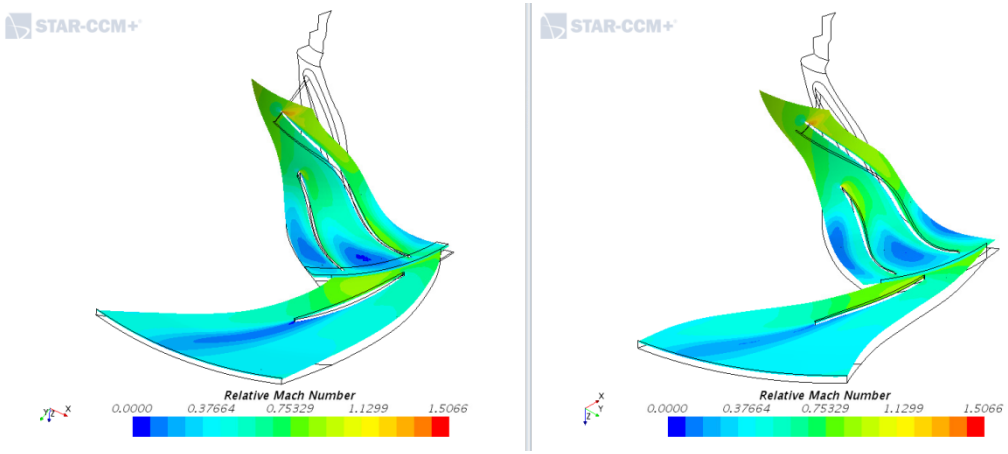


***Figure 17.*** *Sector analysis of the relative Mach number in the impeller and diffuser at 80% spanwise location, simulated in the design point (OP2-1 for the new design). In-house-compressor on the left, new design on the right.*

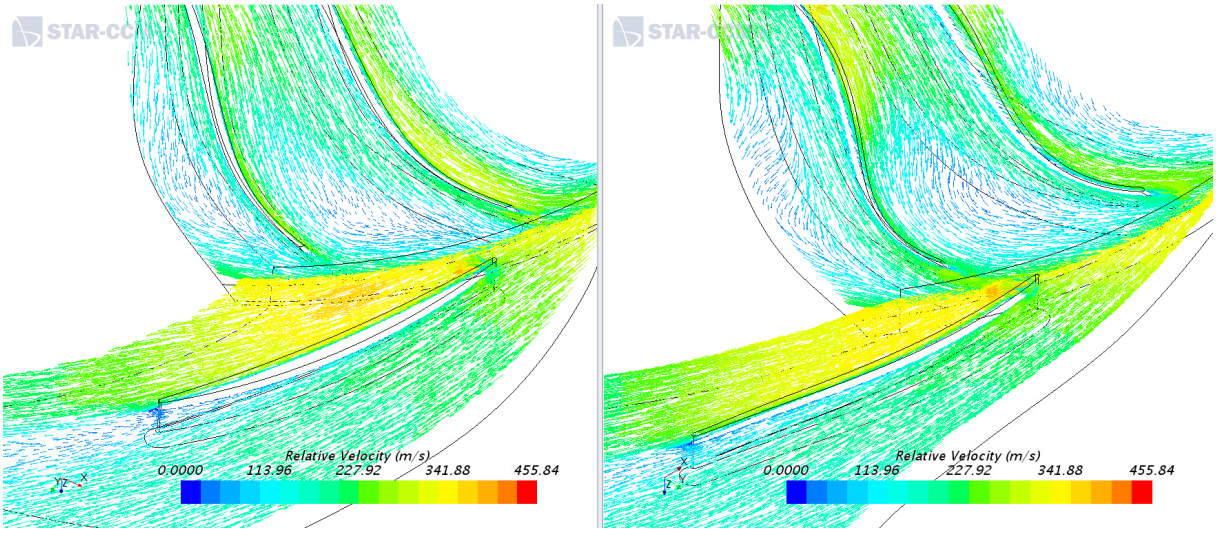


***Figure 18.*** *Sector analysis of the relative velocity vectors in the impeller and diffuser at 80% spanwise location, simulated in the design point (OP2-1 for the new design). In-house-compressor on the left, new design on the right.*

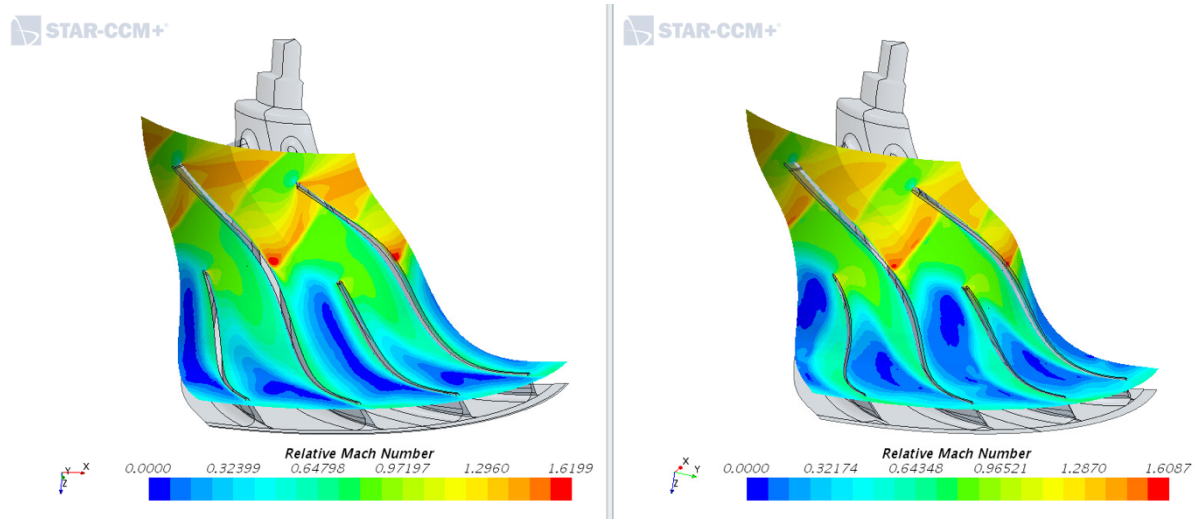


***Figure 19.*** *Sector analysis of the relative Mach number in the impeller at 90 % spanwise location, simulated in OP3. In-house-compressor on the left, new design on the right.*

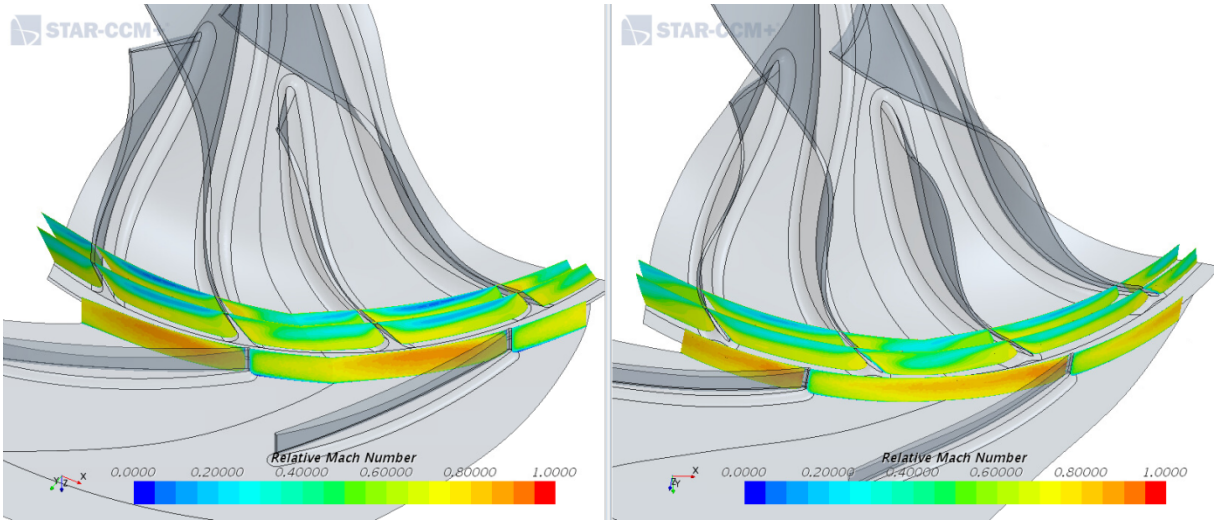


***Figure 20.*** *Sector analysis of the relative Mach number at the diffuser LE, impeller TE, and ~5% upstream from the TE. Simulated in the design point (OP2-1 for the new design). In-house-compressor on the left, new design on the right.*

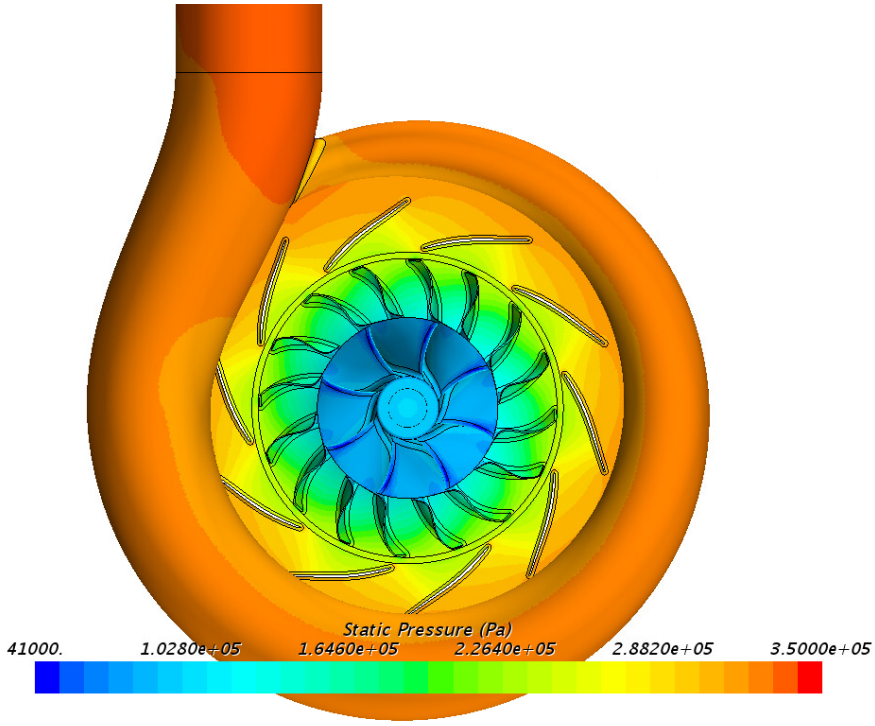


***Figure 21.*** *Static pressure in the impeller, diffuser and volute of the new design.*

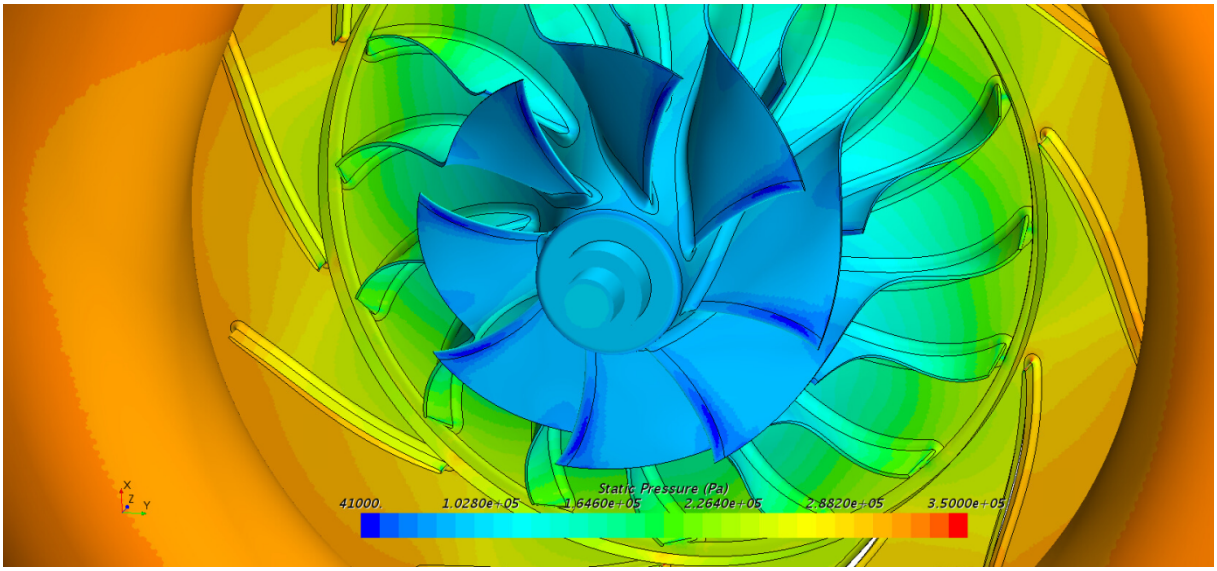


***Figure 22.*** *Detailed view of the static pressure in the impeller and diffuser of the new design.*

# Chapter 5

# Discussion

*The results and their consequences are discussed in this chapter. Suggestions for future work are put forth.*

The exact same operating points could not be simulated for the new design as those for the in-house compressor. This is due to the differences in the two designs; they perform differently. In practice, this means that the pressure ratio and mass flow rate in the simulations of the new design could not both be matched simultaneously to the corresponding values for the in-house-compressor simulations. The idea was therefore to simulate each operating point twice for the new design; once where the mass flow rate was matched to that of the in-house-compressor, and once where the total-to-static pressure ratio at the compressor outlet was matched. This double matching turned out to only be possible in the design point for the full model of the new design. The part load point (OP1) ended up in surge when trying to match to the t/s-ratio (the mass flow rate became too low), and the high load point (OP3) ended up in the choke region when trying to match to the mass flow rate (the mass flow rate became too high). The new design achieved as low flows as the in-house-compressor but not as high; it reached about 97.5% of the flow in the high point. This is partly explained by the smaller throat area of the new design, which is about 95% of the in-house-compressor throat area. It's not only the throat area that determines the choke flow, as indicated by the difference in percentage, but it gives a good indication. Looking at the difference in percent between the high mass flow and throat area, one could speculate that if the new design were given a throat area close to that of the in-house-compressor, then the flow range of the new design may surpass that of the in-house-compressor.
Figure *19* shows that the shock in the inducer is stronger in the in-house-compressor, which supports this argument. The throat area of the new design could be increased by reducing the angle of the blade and meridional hub at the inlet, or the meridional hub radius. However, the latter needs to be followed by a making the impeller blades slightly thicker.

Furthermore, in the high load point the in-house-compressor actually had better efficiency in the diffuser than the new design had, as can be seen in *Table 6*. This could be explained by the fact that the new diffuser has more tangential vanes compared to the in-house-compressor, meaning that the new diffuser is designed for lower flow rates, which causes it to not perform as well at higher flows. The flow range could possibly be somewhat improved by developing the design of the new diffuser further. Only one new diffuser design was created and analyzed due to time constraints, so there is most likely potential in investigating other designs. However, the ambition to increase the flow range in the high region should perhaps not be the

priority, since the in-house-compressor has more operation at lower regions within the map, such as OP1. Therefore, the vanes of the diffuser may perhaps be made even more tangential in order to improve the operation at part loads, which didn't see as big improvements as the design point did.

Examining tables 3-6 it becomes clear that the impeller saw the biggest improvements in efficiency, with a 2.13%-points increase in the part load point (OP1), 2.8%-points and 2.87%-points in the design point (OP2-1 and OP2-2 respectively), and a 3%-points increase in the high point (OP3). The efficiency improvements in the diffuser were conversely not as great, ranging from +0.97%-points in the part load point, +1.83%-points and +1.80%-points in the design point, and displaying an actual decrease of -0.13%-points in the high load point. Looking at the numbers for the complete compressor model, based on the torque, the design point with the matched mass flow rate (OP2-2) had the highest efficiency improvement, one of 1.8%-points.

The improvement of the impeller doesn't seem to carry through to the diffuser and volute, despite the static pressure recovery, $C_p$, in the diffuser being slightly better for the new design compared to the in-house-compressor in all three operating points. One reason for this small improvement in the consequent stages may be due to the lower flow velocities at the impeller exit; the Mach number for the new design is around 2.5% lower compared to the in-house-compressor (in OP2-1). The lower flow velocity entering the diffuser means that the possibility of kinetic energy recovery is lower.

The results under chapter 4.2.1 *Design guidelines* all fall within the stipulated values for what constitutes a "good" design according to Japikse and Korpela.

*Figure 16* and *Figure 17* show that the wake at the trailing edge of the diffuser vane is smaller in the new design than in the in-house-compressor. The relative velocity in the wake is also higher for the new design. This is an improvement since the low flow regime in the wake region acts as a blockage to the core flow.

*Figure 17* and *Figure 18* show that the regions of low flow near the shroud and impeller outlet starts and ends slightly further upstream in the new design compared to the in-house-compressor. The relative velocity of the flow is again higher in the new design. Furthermore, it can be seen in *Figure 19* that this area of low flow has some velocity recovery in the new design, which the in-house-compressor doesn't have. This region of low flow velocity arises due to the curvature of the impeller, which is larger at the shroud than at the hub, this causes a greater adverse pressure gradient at the shroud which leads to a thickening of the boundary layer there (Sundström, 2017). The higher velocity in the new design is therefore once again an improvement, although small.

In *Figure 20* which show the relative Mach number across the flow path at three different streamwise locations around the interface between the impeller and diffuser,

the flow can be seen to be more even in the new design (to the right in the figure). The values for the in-house-compressor reaches higher highs and lower lows compared to the new design.

In the stress and vibration analyses of the new design, the leading edge of the impeller blades were found to be a bit too thin to pass the criterion that Volvo has on the eigenfrequency. The eigenfrequency should be above a certain level so that the blade won't break due to vibrations caused by disturbances in the upstream flow. The criterion that Volvo has on the eigenfrequency is that the blade should be able to withstand vibrations caused by four disturbances in the flow, plus an additional 10%. This is easily amended by increasing the thickness at the leading edge in TD1. This will most likely result in a marginally smaller throat area but means to alleviate this were mentioned above.

The CFD-model of the in-house-compressor was given a smaller tip clearance compared to the real compressor model. This may result in better simulation results compared to if the CFD-model had been given its actual tip clearance. It was helpful to match the tip-clearance of the in-house-compressor to that of the new design in order to definitively say that the improvements were not simply down to the smaller tip clearance, but if one is interested in a more correct comparison, the in-house-compressor should also be simulated with its true tip clearance.

## 5.1 Credibility Analysis

Two additional simulations were done on the complete model of the new design in order to test the resolution of the mesh. The simulations were done in the design point (OP2-1). The "standard" setting that was used had a mesh with a base size of 1.00 mm, ten prism layers with a stretching of 1.6, and a total cell count of 27.2M cells. In the two test simulations the mesh was made coarser and finer respectively. The coarse mesh was given a base size of 1.50 mm, three prism layers with a stretching of 1.5, with a total cell count of 7.4M cells. The fine mesh was in turn given a base size of 0.75mm, ten prism layers with a stretching of 1.6, with a total cell count of 46.49M cells.

The difference in results between the coarse and standard mesh was about 0.82% higher isentropic total-to-total compressor efficiency for the coarse mesh. For the fine mesh the difference was about 0.02% higher compared to the standard mesh. This suggests that the mesh that was used was fine enough, without being too fine in order to achieve reliable results. The finer the mesh the bigger the file size, so it is important to balance the size of the mesh with the size of the file in order to obtain good enough simulation results while minimizing the calculation power needed and thus have efficiency in one's simulations.

Another simulation that tested the choice of turbulence model was also performed. The selected turbulence model of Lag EB (elliptic blending) K-Epsilon was

recommended by Siemens after some discussion over some problems of backflow that arose at the mixing plane between the impeller and diffuser. In the test simulation the SST (Menter) K-Omega turbulence model was selected instead, one that's been used by Volvo previously. The difference in results between the two turbulence models was about 1% higher pressure ratio and compressor efficiency for the K-epsilon model. That model appears to be a bit more forgiving, which was probably why it was recommended in the first place. The results can be considered trustworthy since the same model was used for all simulations for both the in-house-compressor and the new designs. Any deviations or errors arising from the choice of turbulence model will therefore be present in all simulations and are thus of little to no importance from a comparison point-of-view.

CFD-simulation is just a tool; it's not a replacement for real world testing. Therefore, the achieved results should be used as a guide and not as hard facts. That said it is a cost effective and time efficient way of conducting initial evaluations of a new design, especially if that design will be put through several permutations before completion.

## 5.2 Suggestions for Future Work

The new design didn't reach as high choke flow as the in-house-compressor. Since it is meant to function as a replacement it is desirable that the new design should be able to operate within the same regions as the old one. It may therefore be of interest to look into the possibility of further increasing the flow range of the new design and thereby achieving a better replacement option. Suggestions on how to achieve this are:

- To increase the throat area of the impeller, this can be done by reducing the blade inlet angle or the meridional hub angle at the inlet. The meridional hub radius may also be reduced; this should be accompanied by a slight thickening of the impeller blade.
- To adjust the diffuser by turning the diffuser vanes in the radial direction.

Since only one new diffuser design was examined it may be interesting to look into other diffuser design options and how those might perform together with the new impeller design.

Furthermore, the strength of the impeller blades should be improved by increasing the thickness at the leading edge.

# Chapter 6

*The conclusions which answer the problem statement are presented in this chapter.*

## Conclusion

It was possible to achieve better efficiencies with the help of the new tools. The difference was the biggest in the design point, with an increased efficiency of 1.8%-points. The impeller was the part that saw the biggest gain in efficiency, while the diffuser may have further improvement potential by looking into other designs of the diffuser vanes. The choke mass flow of the new design is a bit lower than that of the in-house-compressor. Future work may want to look into the possibility of improving the high-flow capability and blade strength of the new design.

# References


Aungier, R. H., 2000. *Centrifugal Compressors: A Strategy for Aerodynamic Design and Analysis.* 1st ed. New York: ASME Press.

Boles, M. A. & Çengel, Y. A., 2015. *Thermodynamics: An Engineering Approach.* 8th ed. New York: McGraw-Hill Education.

Cohen, H., Rogers, G. & Saravanamuttoo, H., 1996. *Gas Turbine Theory.* 5th ed. Padstow: T. J. Press.

Dickinson, J., 2017. *Vägtrafikens miljöpåverkan.* [Online]
Available at: https://www.naturvardsverket.se/Miljoarbete-i-samhallet/Miljoarbete-i-Sverige/Uppdelat-efter-omrade/Transporter-och-trafik/Vagtrafik/Vagtrafikens-miljopaverkan/
[Accessed 24 May 2018].

Dixon, S. L., 1998. *Fluid Mechanics, Thermodynamics of Turbomachinery.* 4th ed. Oxford: Butterworth-Heinemann.

III, W. G., 2014. *Climate Change 2014 Mitigation of Climate Change,* New York: Cambridge University Press.

International Energy Agency, 2017. *CO2 emissions from fuel combustion - Highlights.* [Online]
Available at:
http://www.iea.org/publications/freepublications/publication/CO2EmissionsfromFuelCombustionHighlights2017.pdf
[Accessed 24 May 2018].

Ising, M., 2017. [Interview] (10 06 2017).

James, 2016. *Volvo History Timeline and List of Current Models.* [Online]
Available at: https://www.globalcarsbrands.com/volvo-history-timeline-and-models-list/
[Accessed 22 May 2018].

Japikse, D., 1996. *Centrifugal Compressor Design and Performance.* 1st ed. Vermont: Concepts ETI, Inc.

Korpela, S. A., 2011. *Principles of Turbomachinery.* 1st ed. Hoboken: John Wiley & Sons, Inc..

Kurz, R. et al., 2016. *Operation of Centrifugal Compressors in Choke Conditions. Paper presented at Asia Turbomachinery and Pump Symposium, Singapore.* San Diego, Texas A&M Engineering Experiment Station .

Lakshminarayana, B., 1996. *Fluid Dynamics and Heat Transfer of Turbomachinery.* 1st ed. Hoboken: John Wiley & Sons, Inc.

Livingston, D., 2000. *documentation.emersonprocess.com.* [Online]
Available at:
http://www.documentation.emersonprocess.com/groups/public/documents/articles_articlesreprints/d350790x012.pdf
[Accessed 26 March 2018].

Sundström, E., 2017. *Flow Instabilities in Centrifugal Compressors at Low Mass Flow Rate,* Stockholm: Universitetsservice US–AB.

United Nations, 1998. *Kyoto Protocol to the United Nations Framework Convention on Climate Change.* Kyoto, United Nations, p. 2.

United Nations, 2015. *Paris Agreement.* Paris, United Nations, p. 3.

University of Southern California, 2018. *USC Libraries.* [Online]
Available at: http://libguides.usc.edu/c.php?g=235034&p=1561756
[Accessed 07 June 2018].

Versteeg, H. & Malalasekera, W., 1995. What is CFD?. In: *An Introduction to Computational Fluid Dynamics: The Finite Volume Method.* Harlow: Pearson Education Limited, p. 1.

Volvo Group, 2018. *Annual and Sustainabilty Report 2017.* [Online]
Available at: http://www.volvogroup.com/content/dam/volvo/volvo-group/markets/global/en-en/investors/reports-and-presentations/annual-reports/annual-and-sustainability-report-2017.pdf
[Accessed 14 May 2018].